Geosci. Model Dev. Discuss., 8, 6217–6266, 2015
www.geosci-model-dev-discuss.net/8/6217/2015/
doi:10.5194/gmdd-8-6217-2015

Geoscientific Model Development Discussions

A global scale mechanistic model of the photosynthetic capacity

A. A. Ali[1,2], C. Xu[1], A. Rogers[3], R. A. Fisher[4], S. D. Wullschleger[5], N. G. McDowell[1], E. C. Massoud[2], J. A. Vrugt[2,6], J. D. Muss[1], J. J. Fisher[7], P. B. Reich[8,9], and C. J. Wilson[1]

[1]Earth and Environmental Sciences Division, Los Alamos National Laboratory, Los Alamos, New Mexico, USA
[2]Department of Civil and Environmental Engineering, University of California Irvine, Irvine, California, USA
[3]Biological, Environmental and Climate Sciences Department, Brookhaven National Laboratory, Upton, New York, USA
[4]Climate and Global Dynamics, National Center for Atmospheric Research, Boulder, Colorado, USA
[5]Climate Change Science Institute, Environmental Sciences Division, Oak Ridge National Laboratory, Oak Ridge, Tennessee, USA
[6]Department of Earth System Science, University of California Irvine, Irvine, California, USA
[7]Jet Propulsion Laboratory, California Institute of Technology, Pasadena, California, USA
[8]Department of Forest Resources, University of Minnesota, St. Paul, Minnesota, USA
[9]Hawkesbury Institute for the Environment, University of Western Sydney, Penrith, New South Wales, Australia

Received: 8 July 2015 – Accepted: 16 July 2015 – Published: 10 August 2015

Correspondence to: C. Xu (xuchongang@gmail.com)

Published by Copernicus Publications on behalf of the European Geosciences Union.

GMDD

8, 6217–6266, 2015

Abstract

Although plant photosynthetic capacity as determined by the maximum carboxylation rate (i.e., $V_{c,max25}$) and the maximum electron transport rate (i.e., J_{max25}) at a reference temperature (generally 25 °C) is known to vary substantially in space and time in response to environmental conditions, it is typically parameterized in Earth system models (ESMs) with tabulated values associated to plant functional types. In this study, we developed a mechanistic model of leaf utilization of nitrogen for assimilation (LUNA V1.0) to predict the photosynthetic capacity at the global scale under different environmental conditions, based on the optimization of nitrogen allocated among light capture, electron transport, carboxylation, and respiration. The LUNA model was able to reasonably well capture the observed patterns of photosynthetic capacity in view that it explained approximately 55 % of the variation in observed $V_{c,max25}$ and 65 % of the variation in observed J_{max25} across the globe. Our model simulations under current and future climate conditions indicated that $V_{c,max25}$ could be most affected in high-latitude regions under a warming climate and that ESMs using a fixed $V_{c,max25}$ or J_{max25} by plant functional types were likely to substantially overestimate future global photosynthesis.

1 Introduction

Photosynthesis is one of the major components of the ecosystem carbon cycle (Canadell et al., 2007; Sellers et al., 1997) and is thus central to Earth system models (ESMs) (Block and Mauritsen, 2013; Hurrell et al., 2013). Most of the ESMs are based on photosynthesis models developed by Farquhar et al. (1980), which are particularly sensitive to photosynthetic capacity. The maximum carboxylation rate scaled to 25 °C (i.e., $V_{c,max25}$ (μmol CO_2 m^{-2} s^{-1})) and the maximum electron transport rate scaled to 25 °C (i.e., J_{max25} (μmol electron m^{-2} s^{-1})) have been generally accepted as the measure of photosynthetic capacity. $V_{c,max25}$ and J_{max25} are the key biochemical parameters in the photosynthesis models as they control the carbon fixation process (Farquhar

GMDD
8, 6217–6266, 2015

et al., 1980). There exist large variations in estimates of gross primary productivity in space and time across ESMs (Schaefer et al., 2012), which have been partly attributed to uncertainties in $V_{c,max25}$ (Bonan et al., 2011). Accurate estimations of $V_{c,max25}$ and J_{max25} are needed to simulate gross primary productivity because errors of $V_{c,max25}$ and J_{max25} may be exacerbated when upscaling from leaf to ecosystem level (Hanson et al., 2004).

Our ability to make reliable predictions of $V_{c,max25}$ and J_{max25} at a global scale is limited. One of the reasons is that we do not have a complete understanding of the processes influencing $V_{c,max25}$ and J_{max25} (Maire et al., 2012; Xu et al., 2012) despite the fact that $V_{c,max25}$ has been measured and studied more extensively than many other photosynthetic parameters (Kattge and Knorr, 2007; Leuning, 1997; Wullschleger, 1993). Many empirical studies have shown that $V_{c,max25}$ and J_{max25} (or field-based surrogates) correlate with leaf nitrogen content (Medlyn et al., 1999; Prentice et al., 2014; Reich et al., 1998; Ryan, 1995; Walker et al., 2014). Therefore, a constant relationship between the leaf nitrogen content and $V_{c,max25}$ or J_{max25} is commonly utilized by many ecosystem models (Bonan et al., 2003; Haxeltine and Prentice, 1996; Kattge et al., 2009). The relationship between leaf nitrogen content, $V_{c,max25}$ and J_{max25} varies with different light, temperature, nitrogen availability and CO_2 conditions (Friend, 1991; Reich et al., 1995; Ripullone et al., 2003), and therefore, the prescribed relationship of $V_{c,max25}$, J_{max25} and leaf nitrogen content might introduce significant biases into predictions of future photosynthetic rates, and also the downstream carbon cycle and climate processes that are dependent on these predictions (Bonan et al., 2011; Knorr and Kattge, 2005; Rogers, 2014).

To better account for the relationships between photosynthetic capacities and their environmental determinants, we developed a mechanistic model of leaf utilization of nitrogen for assimilation (LUNA V1.0) at the global scale that accounts for the key drivers (temperature, radiation, humidity, CO_2 and day length) contributing to the variability in the relationship between leaf nitrogen, $V_{c,max25}$ and J_{max25}. Based on the theoretically optimal amount of leaf nitrogen allocated to different processes, the LUNA model

GMDD
8, 6217–6266, 2015

predicts $V_{c,max25}$ and J_{max25} under different environmental conditions. We estimate the LUNA model parameters by fitting the model predictions to observations of $V_{c,max25}$ and J_{max25}. In order to assess the impacts of future climate change on photosynthesis, we used the calibrated LUNA model to estimate the summer season net photosynthetic rate using predicted $V_{c,max25}$ and J_{max25} under historical and future climate conditions.

2 Methodology

2.1 Overview

Our LUNA model (version 1.0) is based on the nitrogen allocation model developed by Xu et al. (2012), which optimizes nitrogen allocated to light capture, electron transport, carboxylation, and respiration. Xu et al. (2012) considered a series of assumptions on the model to generate optimized nitrogen distributions, these were (i) that storage nitrogen is allocated to meet requirements to support new tissue production; (ii) respiratory nitrogen is equal to the demand implied by the sum of maintenance respiration and growth respiration; (iii) light capture, electron transport and carboxylation are co-limiting to maximize photosynthesis. Xu et al. (2012)'s model need to be calibrated, and has thus far been tested for three test sites. Here, we expand on the work of Xu et al. (2012) to allow global predictions of nitrogen allocation, by fitting the model parameters to an expanded photosynthetic capacity data set. To make global predictions feasible, we also made important refinements to Xu et al. (2012)'s model by considering the impacts of both day length and humidity, and the variations in the balance between light-limited electron transport rate and the Rubisco-limited carboxylation rate in accordance with recent theory. We used an efficient Markov Chain Monte Carlo simulation approach, the Differential Evolution Adaptive Metropolis Snooker Updater (DREAM-ZS) algorithm (Laloy and Vrugt, 2012), to fit the nitrogen allocation model to a large dataset of observed $V_{c,\,max}$ and J_{max} collected across a wide range of environmental gradients (Ali et al., 2015). After model fitting, a sensitivity analysis was

GMDD
8, 6217–6266, 2015

performed to gauge the response of the model to parametric variation and to environmental drivers (temperature, photosynthetic active radiation, day length, relative humidity and atmospheric CO_2 concentration). Finally, using climate projections from the Community Climate System Model (CCSM), mean summer-season $V_{c,max25}$ and J_{max25} and their impacts on net photosynthesis were estimated for the globe.

2.2 Model description

The structure of LUNA model is based on Xu et al. (2012), where plant leaf nitrogen is divided into four pools: structural nitrogen, photosynthetic nitrogen, storage nitrogen and respiratory nitrogen. We assume that plants optimize their nitrogen allocation to maximize the photosynthetic carbon gain, defined as the gross photosynthesis (A) minus the maintenance respiration for photosynthetic enzymes (R_{psn}), under specific environmental conditions and given the leaf nitrogen use strategy determined by four parameters in the LUNA model. These four parameters include (1) $J_{max}b0$ (unitless) specifies baseline proportion of nitrogen allocated for electron transport rate; (2) $J_{max}b1$ (unitless) determines electron transport rate response to light; (3) $t_{c,j0}$ (unitless) specifies the baseline ratio of Rubisco-limited rate to light-limited rate; and (4) H (unitless) determines electron transport rate response to relative humidity. A complete description of the LUNA model and the detailed associated optimization algorithms are provided in Appendix A. This optimality approach was introduced and tested by Xu et al. (2012) for only three test cases, and here we assess its fidelity at large spatial scale with improvement to account for large scale variability. Optimal approaches are an important tool of land surface models, in that they provide a specific testable hypothesis for plant function (Dewar, 2010; Franklin et al., 2012; Schymanski et al., 2009; Thomas and Williams, 2014).

GMDD
8, 6217–6266, 2015

2.3 Data and temperature response functions

Details of data collection are stated in Ali et al. (2015). We used all of the data from Ali et al. (2015) with the exception of one study that collected seasonal data on $V_{c,max}$ and J_{max} during prolonged drought (Xu and Baldocchi, 2003), in view that our model only consider the optimal nitrogen allocation based on the monthly climate conditions but did not consider the potential enzyme deterioration due to long-term droughts. In summary, we used 766 data points for $V_{c,max}$ and 643 data points for J_{max} ranging from tropics to the arctic with a total of 125 species.

To allow comparisons of $V_{c,max}$ and J_{max} data collected at different temperatures, we first standardized data to a common reference temperature (25 °C). To do this, we employed temperature response functions (TRFs). Because of issues related to the possibility of acclimation to temperature, the appropriate TRF to use is not yet a matter of scientific agreement (Yamori et al., 2006). To test the potential impact of our decision on the outcome of the study, we used two alternative temperature response functions in this study. The first temperature response function (TRF1) used Kattge & Knorr's (2007)'s algorithm, which empirically accounts for the potential for acclimation to growth temperature. Following the Community Land Model version 4.5, the growth temperature is constrained between 11 and 35 °C (Oleson et al., 2013) to limit the extent of acclimation to growth temperatures found in the calibration data set. The second temperature response function (TRF2) did not consider change in temperature response coefficients to growth temperature (Kattge and Knorr, 2007). See Appendix B for details of TRF1 and TRF2.

Because LUNA model is based on the C_3 photosynthetic pathway, in this study, we only consider C_3 species. Typically, plant species are grouped into several simple plant functional types (PFTs) in ESMs because of computational limitations and gaps in the ecological knowledge. In view that the processes considered in LUNA model are universal across all C_3 species and limited coverage of environmental conditions for

GMDD
8, 6217–6266, 2015

individual plant functional types, our LUNA model does not differentiate among PFTs for C_3 species. Namely, we have a single model for all C_3 PFTs.

2.4 Parameter estimation

The four parameters in the LUNA model are difficult to measure in the field. In this study, we estimate these parameters by fitting out model against observations of $V_{c,max25}$ and J_{max25} data using the Differential Evolution Adaptive Metropolis (DREAM$_{(ZS)}$) method (Vrugt et al., 2008, 2009; Laloy and Vrugt, 2012). We used the DREAM$_{(ZS)}$ algorithm (Vrugt et al., 2008, 2009; Laloy and Vrugt, 2012) to calibrate our model because this method uses differential evolution (Storn and Price, 1997) as genetic algorithm for population evolution with a Metropolis selection rule to decide whether candidate points should replace their parents or not. This simple MCMC method exhibits excellent sampling efficiencies on a wide range of model calibration problems, including multimodal and high-dimensional search problems. A detailed description of DREAM$_{(ZS)}$ appears in Vrugt et al. (2008, 2009) and Laloy and Vrugt (2012) and interested readers are referred to these publications. A simple Gaussian likelihood function (No.4 in DREAM$_{(ZS)}$) was used to compare our model simulations of $V_{c,max25}$ and J_{max25} with their observed counterparts. Examples of convergence of the parameters are presented in Figs. S1 and S2 in the Supplement.

2.5 Model evaluations

In this study, we considered two statistical metrics to analyze the performance of the LUNA model against the $V_{c,max}$ and J_{max} data. They are the coefficient of determination (r^2) and the model efficiency (ME) (Whitley et al., 2011). The r^2 is estimated using the linear regression model for observed values vs. the predicted values. It measures the proportion of variance in $V_{c,max}$ or J_{max} data explained by the model. The model

GMDD
8, 6217–6266, 2015

efficiency is given as

$$\mathrm{ME} = 1 - \frac{\sum (y_i - \hat{y}_i)^2}{\sum (y_i - \overline{y})^2} \quad (1)$$

where y_i are observations, $\hat{y}_i$ are model estimates and $\overline{y}$ is the mean of observations. It estimates the proportion of variance in the $V_{c,}$max or J_{max} data explained by the 1 : 1 line between model predictions and observations (Mayer and Butler, 1993; Medlyn et al., 2005). The ME can range between 0 and 1, where a ME = 1 corresponds to a "perfect" match between modelled and measured data and a ME = 0 indicates that the model predictions are only as accurate as the mean of the measured data.

2.6 Model sensitivity analysis

We conducted two sensitivity analyses of our model to identify the importance of the model parameters and the environmental variables. In the first sensitivity analysis, each value of the model parameter (J_{maxb0}, J_{maxb1}, $t_{c,j0}$, and H) was perturbed, one at a time, by ±15 % of their fitted values, to measure the importance of model parameters to modeled $V_{c,max25}$ and J_{max25}. In the second sensitivity analysis, the environmental variables (day length (hours), daytime radiation ($\mathrm{W\,m^{-2}}$), temperature (°C), relative humidity (unitless), and carbon dioxide (ppm)) were perturbed, one at a time, by ±15 % of their mean values to identify which environmental variable was most likely to drive modeled $V_{c,max25}$ and J_{max25}.

2.7 Changes in $V_{c,max25}$ and J_{max25} under future climate projections

Global surface temperature by year 2100 (relative to present day) could increase by 3.9 °C (Friedlingstein et al., 2014), with large spatial variations across different regions of the globe (Raddatz et al., 2007). Given the dependence of photosynthesis on temperature, it is critical to examine how much future photosynthesis is likely to change

GMDD
8, 6217–6266, 2015

in different regions. In this study, we aim to investigate the importance of changes in $V_{c,max25}$ and J_{max25} as predicted by the LUNA model to the net photosynthesis rate (A_{net}) estimation in future. The importance is measured by the percentage difference in the estimation of future mean A_{net} for the top canopy leaf layer during the summer season by using $V_{c,max25}$ and J_{max25} estimated for historical climate conditions or the $V_{c,max25}$ and J_{max25} estimated for future climate conditions (See Appendix C for details of A_{net} calculation).

We used Coupled Climate Carbon Cycle Model Intercomparison Project Phase 5 (CMIP5) (Meehl et al., 2000) model outputs to obtain projections of the future climate. Climate modelers have developed four representative concentration pathways (RCPs) for the 21st century that correspond to different amounts of greenhouse gas emissions (Taylor et al., 2013). In this study, we used the historical and future climate conditions simulated by the CCSM 4.0 model under the emission scenario of RCP8.5, which considers the largest greenhouse gas emissions. We did not consider other models and emission scenarios because our main purpose is to estimate the potential impact of our nitrogen allocation model on photosynthesis estimation but not to do a complete analysis under all CMIP5 output. Specifically, we used ten-year climate conditions between 1995 and 2004 for historical and the ten-year climate conditions between 2090 and 2099 for future. We present optimal $V_{c,max25}$ and J_{max25} predictions for the peak growing season months. Data from the NOAA Earth System Research Laboratory over the years 1950 to 2010 (Riebeek, 2011) showed that the maximum amount of carbon dioxide drawn out of the atmosphere occurs in August and February by the large land masses of Northern and Southern Hemisphere, respectively. As a result, June, July and August months were used in this study as the summer season for Northern Hemisphere and December, January and February months were considered as the summer season for the Southern Hemisphere. $V_{c,max25}$ and J_{max25} were predicted using the average values of the climate variables for June, July, August and December, January and February for Northern, Southern Hemispheres, respectively.

GMDD
8, 6217–6266, 2015

In order to identify the importance of changes in different climate variables (temperature, CO_2, radiation and relative humidity) to modeled changes in $V_{c,max25}$ and J_{max25} in the future, we conducted a sensitivity analysis of the impact of changes in climate variables on model results. Specifically, we measured the importance of changes in a specific climate variable by the difference in $V_{c,max25}$ and J_{max25} predicted by the LUNA model driven by historical values or future values of the specific climate variable of interest with all other climate variables set as their historical values.

3 Results

3.1 Model-data comparison of $V_{c,max25}$ and J_{max25}

The DREAM inversion approach allowed us to estimate the four parameters in our *LNUE* model (Table 1). Using the fitted model parameters, the LUNA model explained 54 % of the variance of observed $V_{c,max25}$ across all of the species (Fig. 1a) and 65 % of the variance in observed J_{max25} (Fig. 1b) using temperature response function TRF1 (a temperature response function that considered the potential of acclimation to growth temperature). When temperature response function TRF2 (a temperature response function that did not consider change in temperature response coefficients to growth temperature) was used, the LUNA model explained 57 % of variance in observed $V_{c,max25}$ (Fig. 1c) and 66 % of the variance in observed J_{max25} (Fig. 1d) across all of the species. By comparing the model predictions with only the studies that reported seasonal cycles of $V_{c,max25}$ and J_{max25}, we found the model explained 67 and 53 % of the variance in observed $V_{c,max25}$ and J_{max25}, respectively, when TRF1 was used (Fig. S3a and b in the Supplement). The model explained 67 and 54 % of the variance in observed $V_{c,max25}$ and J_{max25}, respectively, when TRF2 was used (Fig. S3c and d).

Our model also performed well for different PFTs. When using TRF1, for herbaceous plants, the LUNA model explained about 57 % of the variance in observed $V_{c,max25}$ (Fig. S4a). The model explained about 58 and 47 % of the variance in observed $V_{c,max25}$

GMDD
8, 6217–6266, 2015

for shrubs (Fig. S4b) and for trees (Fig. S4c), respectively. For the electron transport, the LUNA model explained about 49, 85 and 46 % of the variances in observed J_{max25} for herbaceous plants (Fig. S4d), shrubs (Fig. S4e) and trees (Fig. S4f), respectively.

When we used a fixed temperature response curve under different growth temperatures (TRF2), for shrubs, the LUNA model has a higher predictive power (about 63 % of the variances in observed $V_{c,max25}$ (Fig. S5b)). Across TRF1 and TRF2, the LUNA model explained similar amount of variance in observed $V_{c,max25}$ for herbaceous and trees (Fig. S5a and c). For J_{max25}, the LUNA model explained a similar amount of variability for herbaceous, shrubs and trees for TRF1 (Fig. S4d–f) and TRF2 (Fig. S5d–f).

3.2 Model sensitivity analysis

Sensitivity analysis of the four model parameters (Table 1) showed that all the four parameters had positive effects on $V_{c,max25}$ (Fig. 2a and c) and J_{max25} (Fig. 2b and d) regardless of the temperature response function used. t_{c,j_0} had the strongest effect on $V_{c,max25}$ (Fig. 2a and c) while $J_{max}b0$ had the strongest effect on J_{max25} (Fig. 2b and d). H had little impact on either $V_{c,max25}$ and J_{max25} (Fig. 2a–d).

Sensitivity analysis of the climate variables showed that, under both temperature response functions (TRF1 and TRF2), the key drivers of change in $V_{c,max25}$ were radiation, day length, temperature, CO_2 and relative humidity in order of decreasing importance (Fig. 3a and c). For J_{max25}, the main drivers of change in J_{max25} were day length, temperature, radiation, relative humidity and CO_2 in order of decreasing importance (Fig. 3b and d), irrespective of which temperature response functions were used.

3.3 Impacts of climate change on $V_{c,max25}$ and J_{max25}

Across the globe, the gradient of $V_{c,max25}$ and J_{max25} is similar irrespective of whether TRF1 or TRF2 was used (Figs. 4 and S6). Under historical conditions, regions from higher latitudes are predicted to have relatively high $V_{c,max25}$ and J_{max25} while lower latitudes are predicted to have relatively low $V_{c,max25}$ and J_{max25} (Fig. 4a and c for TRF1;

GMDD
8, 6217–6266, 2015

Fig. S6a and c for TRF2). Future climatic conditions are likely to decrease $V_{c,max25}$ in many continents mainly due to the predicted increase in temperature and CO_2 concentration (Fig. 4b for TRF1; Fig. S6b for TRF2). J_{max25} is predicted to decrease at higher latitudes but slightly increasing at lower latitudes (Fig. 4d for TRF1and Fig. S6b for TRF2).

Our results showed that $V_{c,max25}$ was most sensitive to CO_2, temperature, radiation and relative humidity in order of decreasing importance (Fig. 5a–d for TRF1 and Fig. S7a–d for TRF2). J_{max25} was most sensitive to temperature, radiation, relative humidity and CO_2 in order of decreasing importance (Fig. 6a–d for TRF1 and Fig. S8a–d for TRF2). Across the globe, temperature had negative impacts on $V_{c,max25}$ when using TRF1 (Fig. 5a); however, $V_{c,max25}$ was found to be increasing at the lower latitudes when using TFR2 (Fig. S7a).

Our model showed that the future summer-season mean photosynthetic rate at the top leaf layer could be substantially overestimated if we does not consider the acclimation of $V_{c,max25}$ and J_{max25} for the future (i.e., using the $V_{c,max25}$ and J_{max25} estimated for historical climate conditions) (Fig. 7a and b), especially for regions with high temperatures (Fig. S9). Compared to the model using TRF1, the overestimation of future summer-season mean photosynthesis rates is much higher than the model using TRF2 (Fig. 7b). The overestimation of total global net photosynthetic rate is 10.1 and 16.3 % for TRF1 and TRF2, respectively.

4 Discussion

4.1 Model limitations

The assumption that nitrogen is allocated according to optimality principles explained a large part of variability in $V_{c,max25}$ (approximately 55 %) and in J_{max25} (approximately 65 %) at the global scale, regardless of the temperature response functions used. It also well captured the seasonal cycles and the PFT-specific values of $V_{c,max25}$ and

GMDD
8, 6217–6266, 2015

J_{max25} (Figs. S3–5). These results suggest our model is able to capture many of the key components of the drivers of $V_{c,max25}$ and J_{max25} across the globe both in space as well as in time. The remaining portion of uncertainty that cannot be explained by our LUNA model could be related to variability within the 125 species considered in this study. Data availability limited the number of species considered and favored the universal LUNA that we used as separate species normally did not cover a large range of environmental conditions; however, we should be able to fit our model to specific PFTs when additional data become available that provides more complete coverage of environmental conditions and PFTs. We expect that such a model would be able to capture more of the variability observed in $V_{c,max25}$ and J_{max25}.

Unexplored nutrient limitations and other plant physiological properties could also play a factor in the limitation of our model. For example, the nitrogen use efficiency of tropical plants (typically modest to low nitrogen) can be diminished by low phosphorus (Cernusak et al., 2010; Reich and Oleksyn, 2004; Walker et al., 2014), suggesting that our model could be improved by considering multiple nutrient limitations (Goll et al., 2012; Wang et al., 2010). Our treatment of photosynthetic capacity could also be improved by incorporating species-specific mesophyll and stomatal conductance (Medlyn et al., 2011), by analyzing leaf properties such as leaf life span (Wright et al., 2004), or by considering soil nutrient and soil water availability.

Another potential reason why the model is unable to explain a significant part of uncertainty in the observation is due to that fact that the measurement error on $V_{c,max25}$ and J_{max25} is rarely reported in the literature. Measurement errors on $V_{c,max25}$ and J_{max25} could result from many sources. Firstly, through different statistical fitting approaches used to fit the Farquhar et al. model (Dubois et al., 2007; Manter and Kerrigan, 2004) to determine the transition C_i value (the value of C_i used to differentiate between Rubisco and RUBP limitations), which are not yet consistent in the literature (Miao et al., 2009). Secondly, obtaining accurate or biologically realistic estimates of dark respiration is often challenging (but see Dubois et al., 2007), and as such, dark respiration is sometimes not reported (Medlyn et al., 2002b).

GMDD
8, 6217–6266, 2015

4.2 Importance of environmental control on $V_{c,max25}$ and J_{max25}

Our model predicts that higher temperatures generally lead to lower values of $V_{c,max25}$ and J_{max25} (Fig. 3a and c). As temperature increases, the nitrogen use efficiencies of $V_{c,max}$ and J_{max} also increase and thus plants need a lower amount of nitrogen allocated for carboxylation and electron transport. This is true for all the sites except for $V_{c,max25}$ in the hotter regions when TRF2 was used (Fig. S7a). The reason is because LUNA model will use a higher increase in night-time temperature (e.g., 22 to 30 °C) than daytime temperature (e.g., from 31 to 33 °C) as constrained by the maximum temperature for optimization in TRF2 (i.e., 33 °C). Thus, the nitrogen use efficiency of daily respiration increases much strongly than the nitrogen use efficiency of $V_{c,max}$. Photosynthesis and respiration is balanced within the model, so plants do not need to invest a lot of nitrogen in respiratory enzymes under hot regions. Therefore, more nitrogen is available for other processes, and the proportion of nitrogen allocated to carboxylation and thus $V_{c,max25}$ increased accordingly.

Our model predicts that CO_2 has negligible effects on J_{max25}, which is supported by reports from other studies (e.g. Maroco et al., 2002). A meta-analysis of 12 FACE experiments indicated reductions of J_{max} of approximately 5 % but a 10 % reduction in $V_{c,max25}$ under elevated CO_2 (Long et al., 2004). Our model also predicts that relative humidity has little effect on $V_{c,max25}$. This may be due to the fact that most of the values of $V_{c,max25}$ and J_{max25} used in our dataset were reported with relatively high humidity values. But, our model, may have underestimated the effects of prolonged drought on $V_{c,max25}$ under low humidity conditions (Xu and Baldocchi, 2003), which we did not consider. Under prolonged drought, plants close their stomata and photosynthesis is greatly reduced (Breshears et al., 2008; McDowell, 2011). Without carbon input and high temperatures during drought, photosynthetic enzymes may degenerate, which could decrease $V_{c,max25}$ substantially (Limousin et al., 2010; Xu and Baldocchi, 2003).

GMDD
8, 6217–6266, 2015

4.3 Importance of changes in $V_{c,max25}$ and J_{max25} to future photosynthesis estimation

Our model suggests that most regions of the world will likely have reductions in $V_{c,max25}$ (Figs. 4b and S6b), because higher temperature (Fig. S10) coupled with elevated CO_2 will increase nitrogen use efficiency of Rubisco and thus plants are able to reduce the amount of nitrogen allocated for Rubisco to reduce the carbon cost required for enzyme maintenance. Similarly, J_{max25} will also decrease globally, except in regions where the present growing temperatures are high (Fig. S9b). The increase of J_{max25} can be attributed to leaf temperature limitation and increased shortwave radiation. Temperature will have little impact on nitrogen allocation in regions with historically high growing temperatures because leaf temperature in already close to or high than the upper limit of optimal nitrogen allocation (42 °C for TRF1 and 33 °C for TRF2). Based on Eq. (A11), higher levels of shortwave solar radiation will increase nitrogen allocation to electron transport (Evans and Poorter, 2001).

If we do not account for the potential acclimation of $V_{c,max25}$ and $V_{c,max25}$ under future climate conditions as predicted by the LUNA model, our analysis indicates that ESM predictions of future global photosynthesis at the uppermost leaf layer will likely be overestimated by as much as 10–14 % if $V_{c,max25}$ and J_{max25} are held fixed (Fig. 7). Therefore, to reliably predict global plant responses to future climate change, ESMs should incorporate models that use environmental control on $V_{c,max25}$ and J_{max25}. It has been recently suggested that nitrogen-related factors are not well represented in ESMs (Houlton et al., 2015; Wieder et al., 2015). Our nitrogen partitioning scheme would help alleviate biases into the predictions of future photosynthetic rates, and also climate processes that are dependent on these predictions (Bonan et al., 2011; Knorr and Kattge, 2005; Rogers, 2014).

GMDD
8, 6217–6266, 2015

Appendix A: Leaf Utilization of Nitrogen for Assimilation (LUNA) Model

The LUNA model considers nitrogen allocation within a given leaf layer in the canopy that has a predefined leaf-area-based plant leaf nitrogen availability (LNC_a; $gN\,m^{-2}$ leaf) to support its growth and maintenance. The structure of the LUNA model is adapted from Xu et al. (2012), where the plant nitrogen at the leaf level is divided into four pools: structural nitrogen (N_{str}; $gN\,m^{-2}$ leaf), photosynthetic nitrogen (N_{psn}; $gN\,m^{-2}$ leaf), storage nitrogen (N_{store}; $gN\,m^{-2}$ leaf), and respiratory nitrogen (N_{resp}; $gN\,m^{-2}$ leaf). Namely,

$$LNC_a = N_{psn} + N_{str} + N_{store} + N_{resp}. \quad \text{(A1)}$$

The photosynthetic nitrogen, N_{psn}, is further divided into nitrogen for light capture (N_{lc}; $gN\,m^{-2}$ leaf), nitrogen for electron transport (N_{et}; $gN\,m^{-2}$ leaf), and nitrogen for carboxylation (N_{cb}; $gN\,m^{-2}$ leaf). Namely,

$$N_{psn} = N_{et} + N_{cb} + N_{lc}. \quad \text{(A2)}$$

The structural nitrogen, N_{str}, is calculated as the multiplication of leaf mass per unit area (LMA: g biomass/m^2 leaf), and the structural nitrogen content (SNC: $gN\,g^{-1}$ biomass). Namely,

$$N_{str} = SNC \cdot LMA \quad \text{(A3)}$$

where SNC is set to be fixed at 0.002 ($gN\,g^{-1}$ biomass), based on data on C : N ratio from dead wood (White et al., 2000). The functional leaf nitrogen content (FNC_a; $gN\,m^{-2}$ leaf) is defined by subtracting structural nitrogen content, N_{str}, from the total leaf nitrogen content (LNC_a; $gN\,m^{-2}$ leaf),

$$FNC_a = LNC_a - N_{str} \quad \text{(A4)}$$

GMDD
8, 6217–6266, 2015

We assume that plants optimize their nitrogen allocations (i.e., $N_{store}, N_{resp}, N_{lc}, N_{et}, N_{cb}$) to maximize the photosynthetic carbon gain, defined as the gross photosynthesis (A) minus the maintenance respiration for photosynthetic enzymes (R_{psn}), under specific environmental conditions and given plant's strategy of leaf nitrogen use. Namely, the solutions of nitrogen allocations $\{N_{store}, N_{resp}, N_{lc}, N_{et}, N_{cb}\}$ can be estimated as follows,

$$\left\{\hat{N}_{store}, \hat{N}_{resp}, \hat{N}_{lc}, \hat{N}_{et}, \hat{N}_{cb}\right\} = \underset{N_{store}+N_{resp}+N_{lc}+N_{et}+N_{cb}<FNC_a}{\operatorname{argmax}} (A - R_{psn}). \quad \text{(A5)}$$

The gross photosynthesis, A, was calculated with a coupled leaf gas exchange model based on the Farquhar et al. (1980) model of photosynthesis and Ball–Berry-type stomatal conductance model (Ball et al., 1987) (See Appendix C for details). The maintenance respiration for photosynthetic enzymes, R_{psn}, is calculated by the multiplication of total photosynthetic nitrogen (N_{psn}) and the maintenance respiration cost for photosynthetic enzyme (NUE_{rp}, see Appendix D). Namely,

$$R_{psn} = NUE_{rp} N_{psn}. \quad \text{(A6)}$$

In the LUNA model, the maximum electron transport rate (J_{max}; μmol electron $m^{-2}\,s^{-1}$) is simulated to have a baseline allocation of nitrogen and additional nitrogen allocation to change depending on the average daytime photosynthetic active radiation (PAR; μmol electron $m^{-2}\,s^{-1}$), day length (hours) and air humidity. Specifically, we have

$$J_{max} = J_{max0} + J_{maxb1} f(\text{day length}) f(\text{humidity}) \alpha \text{PAR} \quad \text{(A7)}$$

The baseline electron transport rate, J_{max0}, is calculated as follows,

$$J_{max0} = J_{maxb0} FNC_a NUE_{J_{max}} \quad \text{(A8)}$$

where J_{maxb0} (unitless) is the baseline proportion of nitrogen allocated for electron transport rate. $NUE_{J_{max}}$ (μmol electron $s^{-1} g^{-1}$ N) is the nitrogen use efficiency of J_{max}

GMDD
8, 6217–6266, 2015

(see Eq. D2 for details). $J_{\mathrm{max}b1}$ (unitless) is a coefficient determining the response of the electron transport rate to amount of absorbed light (i.e., αPAR). f (day length) is a function specifies the impact of day length (hours) on J_{max} in view that longer day length has been demonstrated by previous studies to alter $V_{\mathrm{c,max25}}$ and J_{max25} (Bauerle et al., 2012; Comstock and Ehleringer, 1986) through photoperiod sensing and regulation (e.g. Song et al., 2013). Following Bauerle et al. (2012), f (day length) is simulated as follows,

$$f\,(\text{day length}) = \left(\frac{\text{day length}}{12}\right)^2. \tag{A9}$$

f (humidity) represents the impact of air humitidy on J_{max}. We assume that higher humidity leads to higher J_{max} with less water limiation on stomta opening and that low relative humidity has a stronger impact on nitrogen allocation due to greater water limitation. When relative humidity (RH; unitless) is too low, we assume that plants are physiologically unable to reallocate nitrogen. We therefore assume that there exists a critical value of relative humidity ($\mathrm{RH}_0 = 0.25$; unitless), below which there is no optimal nitrogen allocation. Based on the above assumptions, we have

$$f\,(\text{humidity}) = \left(1 - \mathrm{e}^{\left(-H\frac{\max(\mathrm{RH}-\mathrm{RH}_0,0)}{1-\mathrm{RH}_0}\right)}\right), \tag{A10}$$

where H (unitless) specifies the impact of relative humidity on electron transport rate. Replacing Eq. (A7) with Eqs. (A8), (A9) and (A10), we have

$$J_{\mathrm{max}} = J_{\mathrm{max}b0}\mathrm{FNC_a}\mathrm{NUE}_{J_{\mathrm{max}}} + \tag{A11}$$
$$J_{\mathrm{max}b1}\left(\frac{\text{day length}}{12}\right)^2\left(1 - \mathrm{e}^{\left(-H\frac{\max(\mathrm{RH}-\mathrm{RH}_0,0)}{1-\mathrm{RH}_0}\right)}\right)\alpha\mathrm{PAR}$$

GMDD
8, 6217–6266, 2015

The efficiency of light energy absorption (unitless), α, is calculated depending on the amount of nitrogen allocated for light capture, N_{lc}. Following Niinemets and Tenhunen (1997), we have,

$$\alpha = \frac{0.292}{1 + \frac{0.076}{N_{lc} C_b}} \tag{A12}$$

where 0.292 is the conversion factor from photon to electron. C_b is the conversion factor (1.78) from nitrogen to chlorophyll. After we estimate J_{max}, the actual electron transport rate with the daily maximum radiation (J_x) can be calculated using the empirical expression of Smith (1937),

$$J_x = \frac{\alpha \mathrm{PAR}_{max}}{\left(1 + \frac{\alpha^2 \mathrm{PAR}_{max}^2}{J_{max}^2}\right)^{0.5}} \tag{A13}$$

where PAR_{max} ($\mu mol\, m^{-2}\, s^{-1}$) is the maximum photosynthetically active radiation during the day.

Based on Farquhar et al. (1980) and Wullschleger (1993), we can calculate the electron-limited photosynthetic rate under daily maximum radiation (W_{jx}) and the Rubisco-limited photosynthetic rate (W_c) as follows,

$$W_{J_x} = K_j J_x \tag{A14}$$

$$W_c = K_c V_{c,max} \tag{A15}$$

where K_j and K_c as the conversion factors for J_x, $V_{c,max}$ ($V_{c,max}$ to W_c and J_x to W_{J_x}), respectively (see Eqs. C3 and C5 in Appendix C for details of calculation). Based on Xu et al. (2012), Maire et al. (2012) and Walker et al. (2014), we assume that W_c is proportional to W_{J_x}. Specifically, we have

$$W_c = t_{c,j} W_{J_x} \tag{A16}$$

GMDD
8, 6217–6266, 2015

where $t_{c,j}$ is the ratio of W_c to W_{J_x}. We recognize that this ratio may change depending on the nitrogen use efficiency of carboxylation and electron transport (Ainsworth and Rogers, 2007) and therefore introduce the modification as follows,

$$t_{c,j} = t_{c,j0}\left(\frac{\mathrm{NUE_c}/\mathrm{NUE}_j}{\mathrm{NUE_{c0}}/\mathrm{NUE}_{j0}}\right)^{0.5}, \quad \text{(A17)}$$

where $t_{c,j0}$ (unitless) is the ratio of Rubisco-limited rate to light limited rate, $\mathrm{NUE_{c0}}$ (μmol CO_2 $s^{-1}g^{-1}$ N), NUE_{j0} (μmol CO_2 $s^{-1}g^{-1}$ N) are the daily nitrogen use efficiency of W_c and W_j under reference climate conditions defined as the 25 °C leaf temperature and atmospheric CO_2 concentration of 380 ppm, with leaf internal CO_2 concentration set as 70 % of the atmospheric CO_2 concentration. $\mathrm{NUE_c}$ (μmol CO_2 $s^{-1}g^{-1}$ N), NUE_j (μmol CO_2 $s^{-1}g^{-1}$ N) are the nitrogen use efficiency of W_c and W_j at the current climate conditions. See Eqs. (D6) and (D7) for details of calculation. The term $\frac{\mathrm{NUE_c}/\mathrm{NUE}_j}{\mathrm{NUE_{c0}}/\mathrm{NUE}_{j0}}$ determines that the higher nitrogen use efficiency of W_c compared to that of W_j will lead to a higher value of $t_{c,j}$ (or a higher value of W_c given the same value of W_j). The exponent 0.5 was used to ensure that the response of $V_{c,max}$ to elevated CO_2 is down-regulated by approximately 10 % when CO_2 increased from 365 to 567 ppm as reported by Ainsworth and Rogers (2007).

Replacing Eq. (A16) with Eqs. (A14), (A15) and (A17), we are able to estimate the maximum carboxylation rate ($V_{c,max}$; μmol CO_2 m^{-2} s^{-1}) as follows,

$$V_{c,max} = t_{c,j0}\left(\frac{\mathrm{NUE_c}/\mathrm{NUE}_j}{\mathrm{NUE_{c0}}/\mathrm{NUE}_{j0}}\right)^{0.5}\left(\frac{K_j}{K_c}\right)J_x. \quad \text{(A18)}$$

Following Collatz et al. (1991a), the total respiration (R_t) is calculated in proportion to $V_{c,max}$,

$$R_t = 0.015V_{c,max}. \quad \text{(A19)}$$

GMDD
8, 6217–6266, 2015

Accounting for the daytime and nighttime temperature, we are able to estimate the daily respirations as follows,

$$R_{td} = R_t[D_{day} + D_{night} f_r(T_{night})/f_r(T_{day})], \quad \text{(A20)}$$

where D_{day} and D_{night} are daytime and nighttime durations in seconds. $f_r(T_{night})$ and $f_r(T_{day})$ are the temperature response functions for respiration (see Eq. B1 for details).

In summary, given an initial estimation of N_{lc}, we are able to first estimate the efficiency of light energy absorption α using Eq. (A12). With that, we are able to estimate the maximum electron transport rate, J_{max}, using Eq. (A11). The nitrogen allocated for electron transport can thus be calculated as follows,

$$N_{et} = \frac{J_{max}}{NUE_{J_{max}}} \quad \text{(A21)}$$

Then, based on Eq. (A18), we are able to estimate the corresponding the maximum carboxylation rate $V_{c,max}$ and the nitrogen allocated for carboxylation as follows,

$$N_{cb} = \frac{V_{c,max}}{NUE_{V_{c,max}}} \quad \text{(A22)}$$

where $NUE_{V_c,max}$ is the nitrogen use efficiency for $V_{c,max}$. See Eq. (D1) for details of calculation. Using Eq. (A 20), we are able to estimate R_{td} and thus the nitrogen allocated for respiration as follows,

$$N_{resp} = \frac{R_{td}}{NUE_r}, \quad \text{(A23)}$$

where NUE_r is nitrogen use efficiency of enzymes for respiration. See Eq. (D3) for details of calculation. Finally, the "storage" nitrogen is calculated as follows,

$$N_{store} = FNC_a - N_{resp} - N_{cb} - N_{lc} - N_{et}. \quad \text{(A24)}$$

GMDD
8, 6217–6266, 2015

Note that this "storage" nitrogen is mainly a remaining component of FNC_a. Its formulation is different from the formulation of Xu et al. (2012) where N_{store} is set as a linear function of net photosynthetic rate. This modification is based on the observations that the preliminary fitting to data using the linear function shows no dependence of N_{store} on net photosynthetic rate. To make the solutions realistic, we set minimum of N_{store} as 5 % of NC_a in view of potential nitrogen for plant functionality that is not accounted for by photosynthesis and respiration. By exploring different values of nitrogen allocated for light capture N_{lc} and using the Eqs. (A21–23), we will find the "optimal" nitrogen allocations ($\hat{N}_{store}, \hat{N}_{resp}, \hat{N}_{lc}, \hat{N}_{et}, \hat{N}_{cb}$) until the net photosynthetic rate is maximized (see Eq. A5) given a specific set of nitrogen allocation coefficients (i.e., $J_{maxb0} J_{maxb1}, H$, and t_{c,j_0}). The detailed optimization algorithms are implemented as follows:

1. Increase the nitrogen allocated (N_{lc}) for light capture (from a small initial value of 0.05) and calculate the corresponding light absorption rate α with Eq. (A12);
2. Calculate J_{max} from Eq. (A11) and derive the nitrogen allocated to electron transport, N_{et}, using Eq. (A21);
3. Calculate $V_{c,max}$ from Eq. (A18) and derive the nitrogen allocated to Rubisco, N_{cb}, using Eq. (A22);
4. Calculate the total respiration R_{td} from Eq. (A20) and derive the nitrogen allocated to respiration, N_{resp}, using Eq. (A23);
5. Calculate the total nitrogen invest in photosynthetic enzymes including nitrogen for electron transport, carboxylation and light capture using Eq. (A2);
6. Calculate the gross photosynthetic rate, A, and the maintenance respiration for photosynthetic enzymes, R_{psn}, by Eq. (A6);
7. Repeat steps (1) to (6) until the increase from previous time step in A is smaller or equal to the increase in R_{psn}.

GMDD
8, 6217–6266, 2015

Since the response of $V_{c,max}$ and J_{max} to increasing temperature shows a steady rise to an optimum followed by a relatively rapid decline (Bernacchi et al., 2003; Kattge and Knorr, 2007; Leuning, 2002; Medlyn et al., 2002a), we postulate that the detrimental heat stress on leaf enzymatic activity beyond this optimum (Crafts-Brandner and Law, 2000; Crafts-Brandner and Salvucci, 2000; Law and Crafts-Brandner, 1999; Spreitzer and Salvucci, 2002) will cause the leaf to fail to optimize its nitrogen allocation. Consequently, we hypothesized that plants only optimize nitrogen allocation up to their optimum enzymatic activity, which is 42 °C for TRF1 and 33 °C for TRF2. Regardless of whether plants acclimate to temperature or not, we assume that they do not optimally allocate nitrogen when leaf temperature is below 5 °C because low temperatures could substantially limit plant enzymes (Martin et al., 1978; Öquist et al., 1980; Strand and Öquist, 1988).

After we get the optimal nitrogen allocations ($\hat{N}_{store}, \hat{N}_{resp}, \hat{N}_{lc}, \hat{N}_{et}, \hat{N}_{cb}$), we are able to estimate the $V_{c,max25}$ and J_{max25} by rearranging Eqs. (A20) and (A21) as follows,

$$V_{c,max25} = \hat{N}_{cb} NUE_{V_c,max25} \quad \text{(A25)}$$

$$J_{max25} = \hat{N}_{cb} NUE_{Jmax25} \quad \text{(A26)}$$

where $NUE_{V_c,max25}$ and NUE_{Jmax25} are the nitrogen use efficiency for $V_{c,max25}$ and J_{max25}. See Eqs. (D1) and (D2) in Appendix D for details of calculations.

Appendix B: Temperature response functions

Temperature dependence of Rubisco and respiration

The temperature dependence of Rubisco kinetic parameters (K_c, K_o, τ) and mitochondrial respiration in light (R_d) (Farquhar et al., 1980) was an Arrhenius function taken from Bernacchi et al. (2001). The temperature response functions of Rubisco kinetic parameters used are outlined below, which were the same irrespective of whether

GMDD
8, 6217–6266, 2015

plants were assumed to acclimate to growth temperatures (Temperature response function one; TRF1) or not (Temperature response function two; TRF2).

Community land model version 4.5 (CLM4.5) (Oleson et al., 2013) uses the partial pressures of oxygen, O as 20 900 Pa. The kinetic properties of Rubisco which depend on temperature are Rubisco specific factor, τ (Jordan and Ogren, 1984), K_{cc} and K_o, which are the Michaelis–Menten constants for CO_2 and O_2, respectively. The temperature response function of R_d and kinetic properties of Rubisco (K_{cc}, K_o, τ) are described below, where the fixed coefficients of the equations are values at 25 °C.

$$f_r(T_1) = e^{[(46\,390/RT_0)(1-T_0/T_1)]} \quad \text{(B1)}$$

$$K_0(T_1) = 27\,840e^{[(36\,380/RT_0)(1-T_0/T_1)]} \quad \text{(B2)}$$

$$K_c(T_1) = 40.49e^{[(79\,430/RT_0)(1-T_0/T_1)]} \quad \text{(B3)}$$

$$\tau(T_1) = 2407.834e^{[(37\,830/RT_0)(1-T_0/T_1)]} \quad \text{(B4)}$$

In the above equations, R is the universal gas constant (8.314 J mol^{-1} K^{-1}), T_1 is the leaf temperature (K) and the reference temperature, T_0 = 298.15 K.

Temperature dependence of $V_{c,max}$ and J_{max}

Temperature sensitivities of $V_{c,max}$ and J_{max} were simulated using a modified Arrhenius function (e.g. Kattge and Knorr, 2007; Medlyn et al., 2002a; Walker et al., 2014). Because the temperature relationship could acclimate, we examined Kattge and Knorr (2007)'s formulation of with and without temperature acclimation to plant growth temperature. We used two temperature dependence functions of $V_{c,max}$ and J_{max}, which are described below.

Temperature response function one (TRF1)

Fundamentally, TRF1 is a temperature dependence of $V_{c,\,max}$ and J_{max}, which is based on the formulation and parameterization as in Medlyn et al. (2002a) but further modi-

GMDD
8, 6217–6266, 2015

fied by Kattge and Knorr (2007) to make the temperature optima a function of growth temperature (T_g; °C).

$$V_{c,max}(T_1 T_g) = V_{c,max25} f_{V_{c,\,max}}(T_1 T_g) \tag{B5}$$

with

$$f_{V_{c,max}}(T_1, T_g) = \frac{\left(1 + e^{[(S_v T_0 - H_d)/(RT_0)]}\right) e^{[(H_a/RT_0)(1 - T_0/T_1)]}}{1 + e^{[(S_v T_1 - H_d)/(RT_1)]}} \tag{B6}$$

where $V_{c,max25}$ is the value of $V_{c,max}$ at the reference temperature ($T_0 = 298.15\,K$). H_a ($J\,mol^{-1}$) is energy of activation and H_d ($J\,mol^{-1}$) is the energy of deactivation. The entropy term, S_v ($J\,mol^{-1}\,K^{-1}$), is now a function of temperature (Kattge and Knorr, 2007): $S_v = a + bT_g$, where a and b are acclimation parameters for S_v, R is the universal gas constant ($8.314\,J\,mol^{-1}\,K^{-1}$) and the leaf temperature is $T_1(K)$.

TRF1 is implemented in CLM4.5 by Oleson et al. (2013), who uses the form of temperature dependence of $V_{c,max}$ and J_{max} as shown in Eq. (B5), but with limited temperature acclimation, where $S_v = 668.39 - 1.07 \cdot \min(\max(tgrowth, 11), 35)$. Other parameters that are present in CLM4.5 model include, $H_a = 72\,000\,J\,mol^{-1}$ and $H_d = 200\,000\,J\,mol^{-1}$. The values of the acclimation parameters ($a = 668.39$ and $b = -1.07$) were taken from Table 3 of Kattge and Knorr (2007), which were fixed across our data set. The same values of a and b are used by CLM4.5.

A equation similar to Eq. (B6), $f_{J_{max}}(T_1, T_g)$, is used to describe the temperature dependence of J_{max} with the corresponding S_v equation (that considers limited temperature acclimation). The corresponding values of the acclimation parameters (a and b), were again taken from Table 3 of Kattge and Knorr (2007) and were fixed across our data set. The same values of a and b are used by CLM4.5. We used the remaining parameter values as in CLM4.5 that included, $H_a = 50\,000\,J\,mol^{-1}$ and $H_d = 200\,000\,J\,mol^{-1}$.

GMDD
8, 6217–6266, 2015

Temperature response function two (TRF2)

TRF2 does not consider temperature acclimation. The formulation of TRF2 is same as TRF1 except that in TRF2, the entropy term; S_v ($\mathrm{J\,mol^{-1}\,K^{-1}}$) is fixed across our data set. The values of S_v were taken from Table 3 of Kattge and Knorr (2007), which were fixed across our data set. For $V_{c,max25}$, S_v was 649.12 $\mathrm{J\,mol^{-1}\,K^{-1}}$, and for J_{max25}, S_v was 646.22 $\mathrm{J\,mol^{-1}\,K^{-1}}$.

Appendix C: The farquhar photosynthesis and Ball–Berry model

Overview

Photosynthesis is described using a system of three equations and three unknown variables. The three unknown variables include (1) the net rate of leaf photosynthesis (A); (2) stomatal conductance (g_s); and (3) the intercellular partial pressure of CO_2(C_i). All of the unknown factors influence one another. The three equations includes (1) the Farquhar's non-linear equation (A vs. C_i); (2) the Ball–Berry equation (g_s vs. A); and (3) the diffusion equation ($A = g_s\,(C_a – C_i)$). We solved all of these equations simultaneously by taking an iterative approach (Collatz et al., 1991a; Harley et al., 1992; Leuning, 1990). The detailed algorithm for modeling photosynthesis is described below.

Modelling photosynthesis

The photosynthetic rate (A) depends upon (i) the amount, activity, and kinetic properties of Rubisco, and (ii) the rate of ribulose-1,5 bisphosphate (RuBP) regeneration via electron transport (Farquhar et al., 1980). The "minimum" of these two limiting conditions yields the following expression,

$$A = \min\left(W_c, W_j\right) \tag{C1}$$

GMDD
8, 6217–6266, 2015

where W_c is the Rubisco limited rate and W_j is the electron transport limited rate. The Rubisco-limited carboxylation can be described by,

$$W_c = K_c V_{c,max}, \tag{C2}$$

with

$$K_c = \frac{\max(0, C_i - \frac{0.5O}{\tau})}{C_i + K_{cc}\left(1 + O/K_O\right)}, \tag{C3}$$

where $V_{c,max}$ is the maximum rate of carboxylation, competitive with respect to both CO_2 and oxygen, and K_{cc} and K_O are Michaelis constants for carboxylation and oxygenation, respectively. τ is the specificity factor for Rubisco (Jordan and Ogren, 1984), while C_i, and O are the partial pressures of CO_2 and O_2 in the intercellular air space, respectively. Likewise, the electron-limited rate of carboxylation can be expressed by,

$$W_j = K_j J, \tag{C4}$$

with

$$K_j = \frac{\max(0, C_i - \frac{0.5O}{\tau})}{4\left(C_i + 2\frac{0.5O}{\tau}\right)}, \tag{C5}$$

where J is the potential rate of electron transport, and the factor 4 indicates that the transport of four electrons will generate sufficient ATP and NADPH for the regeneration of RuBP in the Calvin cycle (Farquhar and von Caemmerer, 1982). The potential rate of electron transport is dependent upon irradiance, I, according to the empirical expression of Smith (1937),

$$J = \frac{\alpha I}{\left(1 + \frac{\alpha^2 I^2}{J_{max}^2}\right)^{1/2}} \tag{C6}$$

GMDD
8, 6217–6266, 2015

where α, the efficiency of light energy conversion is considered as 0.292 (unitless) (Niinemets and Tenhunen, 1997) and J_{max} is the maximum rate of electron transport.

Ball–Berry model

The stomatal conductance (g, $m\,s^{-1}$) was evaluated by the Ball–Berry empirical stomatal conductance model (Ball et al., 1987):

$$g = g_0 + m\frac{A\mathrm{RH}}{C_a} \tag{C7}$$

where RH is the relative humidity (unitless) at the leaf surface, C_a is the CO_2 concentration at the leaf surface, and g_0 ($0.0005\,s\,m^{-1}$) and m are the maximum stomatal conductance and slope (9, constant across all C_3 species), respectively.

The estimation of A could be sensitive to the choice of maximum stomatal conductance slope, which we set the same for all species, despite the evidence that this parameter varies both within and across species (Harley and Baldocchi, 1995; Wilson et al., 2001). A recent synthesis provides the first analysis of the global variation in stomatal slope based on an alternative algorithm that considers representation of optimal stomatal behavior (Lin et al., 2015). However, following CLM4.5, which uses the Ball–Berry empirical stomatal conductance model (Ball et al., 1987), we fixed the value of stomatal slope (m) as 9 for all PFTs in our study.

Calculation of photosynthesis and stomata conductance

We solved Farquhar's non-linear equation (A vs. C_i), the Ball–Berry equation (g_s vs. A) and the diffusion equation ($A = g_s\,(C_a – C_i)$ simultaneously by taking an iterative approach (Collatz et al., 1991a; Harley et al., 1992; Leuning, 1990) until values of A, g_s, and C_i were obtained. The three equations were solved in two phases; the first phase included solving the equations for which Rubisco was limiting while the second phase considered light limitation. The following steps were followed:

GMDD
8, 6217–6266, 2015

1. Given the initial values of C_i (where initial value of C_i was assumed 0.7 × ambient CO_2 concentration), the temperature dependence functions of $V_{c,max}$ and J_{max} (see Appendix B), and the temperature dependence of Rubisco kinetics (O, τ, K_c and K_O, Appendix B), A was calculated from Eq. (C1).
2. CO_2 concentration at the leaf surface (C_a) was determined by calculating the difference between C_i and the partial pressure due to A, wind speed and the dimension of the leaf.
3. Given A and C_a, and using Eq. (C7), stomatal conductance (g) was determined.
4. C_i was determined by calculating the difference between C_a and partial pressure due to A and boundary conditions of the stomata.
5. Using the leaf energy balance based on absorbed short-wave radiation, molar latent heat content of water vapor, air temperature, and a parameter that governs the rate of convective cooling ($38.4\,J\,m^{-2}\,s^{-1}\,K^{-1}$) (Jarvis, 1986; Moorcroft et al., 2001), leaf temperature was calculated.

The above five steps were repeated in a systematic way until g was equilibrated. The final value of A was then recorded.

Appendix D: Nitrogen use efficiencies

The nitrogen use efficiency for $V_{c,max}$ ($NUE_{V_{c,max}}$, $\mu mol\,CO_2\,g^{-1}\,N\,s^{-1}$) is estimated from a baseline nitrogen use efficiency 25 °C ($NUE_{V_{c,max25}}$) and a corresponding temperature response function at as follows,

$$NUE_{V_{c,max}} = NUE_{V_{c,max25}} \times f_{V_{c,max}}(T, T_g), \quad \text{(D1)}$$

with

$$NUE_{V_{c,max25}} = 47.3 \times 6.25,$$

GMDD
8, 6217–6266, 2015

where the constant 47.3 is the specific Rubisco activity ($\mu mol\, CO_2\, g^{-1}\, Rubisco\, s^{-1}$) measured at 25 °C and the constant 6.25 is the nitrogen binding factor for Rubisco (g Rubisco g^{-1} N) (Rogers, 2014). $f_{V_{c,max}}(T, T_g)$ is the function specifying the temperature dependence of $V_{c,max}$ with T as the leaf temperature and T_g as the growth air temperature (See Appendix B for details of the temperature dependence of $V_{c,\,max}$).

The nitrogen use efficiency for J_{max} ($NUE_{J_{max}}$, μmol electron $g^{-1}\, N\, s^{-1}$) is estimated based on a characteristic protein cytochrome f (Niinemets and Tenhunen, 1997),

$$NUE_{J_{max}} = NUE_{J_{max25}} \times f_{Jmax}(T, T_g) \quad \text{(D2)}$$

with

$$NUE_{J_{max25}} = 8.06 \times 156,$$

where the coefficient 156 is the maximum electron transport rate for cytochrome f at 25 °C (μmol electron μmol cytochrome f); 8.06 is the nitrogen binding coefficient for cytochrome f (μmol cytochrome f g^{-1}N in bioenergetics). $f_{Jmax}(T, T_g)$ is a function specifies the dependence of J_{max} on temperature (See Appendix B for details of the temperature dependence of J_{max}).

The nitrogen use efficiency of enzymes for respiration ($\mu mol\, CO_2\, g^{-1}\, N\, day^{-1}$), NUE_r, is assumed to be temperature-dependent. Specifically, it is calculated as follows,

$$NUE_r = 33.69[D_{day} f_r(T_{day}) + D_{night} f_r(T_{night})] \quad \text{(D3)}$$

where 33.69 is the specific nitrogen use efficiency for respiration at 25 °C ($\mu mol\, CO_2\, g^{-1}\, N\, s^{-1}$) (Makino and Osmond, 1991) and $f_r(T)$ specifies the dependence of respiration on temperature. D_{day} and D_{night} is the daytime and nighttime length in seconds.

The maintenance respiration cost for all photosynthetic enzymes (NUE_{rp}, $\mu mol\, CO_2\, g^{-1}\, N\, s^{-1}$) is calculated as follows:

$$NUE_{rp} = NUE_{rp25} f_r(T, T_g), \quad \text{(D4)}$$

GMDD
8, 6217–6266, 2015

where NUE_{rp25} is the nitrogen use efficiency at 25 °C. NUE_{rp25} is estimated from the observation of J_{max25} and $V_{c,max25}$ as follows,

$$NUE_{rp25} = \frac{0.8 \times 0.5 \times 0.015 \times V_{c,max25}}{\frac{J_{max25}}{NUE_{J_{max25}}} + \frac{V_{c,max25}}{NUE_{V_{c,max25}}} + 0.2}, \quad \text{(D5)}$$

where the total respiration is set as 1.5 % of $V_{c,max}$ (Collatz et al., 1991b). We assume that 50 % of the total respiration is used for maintenance respiration (Van Oijen et al., 2010) and 80 % of the maintenance respiration is used for photosynthetic enzyme. In view that the light absorption rate is generally around 80 % (Niinemets and Tenhunen, 1997), we set the nitrogen for light capture as 0.2 based on Eq. (A12) in Appendix A. $NUE_{J_{max25}}$ and $NUE_{V_{c,max25}}$ are the nitrogen use efficiency for J_{max25} and $V_{c,max25}$ estimated from Eqs. (D1) and (D2). In this study, we used the estimated mean value of 0.715 for NUE_{rp25} based on the data of Ali et al. (2015).

The nitrogen use efficiency for carboxylation (NUE_c) is calculated as the multiplication of conversion factor K_c and the nitrogen use efficiency for $V_{c,max}$ follows:

$$NUE_c = K_c NUE_{V_{c,max}}, \quad \text{(D6)}$$

where K_c is calculated based on the actual internal CO_2 concentrations and leaf temperature (see Eq. C3 for details). Correspondingly, the reference nitrogen use efficiency for carboxylation (NUE_{c0}) is calculated using the Eq. (D5) except that K_c is calculated based on the reference internal CO_2 concentration of 26.95 Pa and the reference leaf temperature of 25 °C. The reference internal CO_2 concentration is estimated by assuming 70 % of the atmospheric CO_2 concentration of 380 ppm and an air pressure of 101 325 Pa.

The nitrogen use efficiency for electron transport (NUE_j) is calculated as the multiplication of conversion factor K_j and the nitrogen use efficiency for J_{max} follows:

$$NUE_j = K_j NUE_{J_{max}}, \quad \text{(D7)}$$

GMDD
8, 6217–6266, 2015

where K_j is calculated based on the actual internal CO_2 concentrations and leaf temperature (see Eq. C5 in Appendix C for details). Correspondingly, the reference nitrogen use efficiency for electron transport (NUE_{j0}) is calculated using the Eq. (D6) except that K_j is calculated based on the reference internal CO_2 concentration of 26.95 Pa and the reference leaf temperature of 25 °C. The reference internal CO_2 concentration is estimated by assuming 70 % of the atmospheric CO_2 concentration of 380 ppm and an air pressure of 101 325 Pa.

Code availability

This model is currently implemented into CLM5.0 and will be released to public when CLM 5.0 is released. Meanwhile, we have code available in the form of MATLAB, FORTRAN and C#. It can be obtained upon request by sending an email to cxu@lanl.gov.

The Supplement related to this article is available online at doi:10.5194/gmdd-8-6217-2015-supplement.

Acknowledgements. This work is funded by UC Lab Research Program (ID: 2012UCLRP0IT00000068990) and by the DOE Office of Science, Next Generation Ecosystem Experiment (NGEE) program in the arctic. This submission is under public release with the approved LA-UR-14-23309.

References

Ainsworth, E. A. and Rogers, A.: The response of photosynthesis and stomatal conductance to rising (CO_2): mechanisms and environmental interactions, Plant Cell Environ., 30, 258–270, 2007.

Ali, A. A., Xu, C., Rogers, A., McDowell, N. G., Medlyn, B. E., Fisher, R. A., Wullschleger, S. D., Reich, P. B., Vrugt, J. A., Bauerle, W. L., Santiago, L. S., and Wilson, C. J.: Global scale environmental control of plant photosynthetic capacity, Ecol. Appl., in press, doi:10.1890/14-2111.1, 2015.

GMDD
8, 6217–6266, 2015

Ball, J. T., Woodrow, I. E., and Berry, J. A.: A model predicting stomatal conductance and its contribution to the control of photosynthesis under different environmental conditions, Springer, Dordrecht, the Netherlands, 221–224, 1987.

Bauerle, W. L., Oren, R., Way, D. A., Qian, S. S., Stoy, P. C., Thornton, P. E., Bowden, J. D., Hoffman, F. M., and Reynolds, R. F.: Photoperiodic regulation of the seasonal pattern of photosynthetic capacity and the implications for carbon cycling, P. Natl. Acad. Sci. USA, 109, 8612–8617, 2012.

Bernacchi, C. J., Singsaas, E. L., Pimentel, C., Portis Jr., A. R., and Long, S. P.: Improved temperature response functions for models of Rubisco-limited photosynthesis, Plant Cell Environ., 24, 253–259, 2001.

Bernacchi, C. J., Pimentel, C., and Long, S. P.: In vivo temperature response functions of parameters required to model RuBP-limited photosynthesis, Plant Cell Environ., 26, 1419–1430, 2003.

Block, K. and Mauritsen, T.: Forcing and feedback in the MPI-ESM-LR coupled model under abruptly quadrupled CO_2, Journal of Advances in Modeling Earth Systems, 5, 676–691, 2013.

Bonan, G. B., Levis, S., Sitch, S., Vertenstein, M., and Oelson, K. W.: A dynamic global vegetation model for use with climate models: concepts and description of simulated vegetation dynamics, Glob. Change Biol., 9, 1543–1566, 2003.

Bonan, G. B., Lawrence, P. J., Oleson, K. W., Levis, S., Jung, M., Reichstein, M., Lawrence, D. M., and Swenson, S. C.: Improving canopy processes in the community land model version 4 (CLM4) using global flux fields empirically inferred from FLUXNET data, J. Geophys. Res., 116, 1–22, 2011.

Breshears, D. D., Myers, O. B., Meyer, C. W., Barnes, F. J., Zou, C. B., Allen, C. D., McDowell, N. G., and Pockman, W. T.: Tree die-off in response to global change-type drought: mortality insights from a decade of plant water potential measurements, Front. Ecol. Environ., 7, 185–189, 2008.

Canadell, J. G., Le Quéré, C., Raupach, M. R., Field, C. B., Buitenhuis, E. T., Ciais, P., Conway, T. J., Gillett, N. P., Houghton, R. A., and Marland, G.: Contributions to accelerating atmospheric CO_2 growth from economic activity, carbon intensity, and efficiency of natural sinks, P. Natl. Acad. Sci. USA, 104, 18866–18870, 2007.

GMDD
8, 6217–6266, 2015

Cernusak, L. A., Winter, K., and Turner, B. L.: Leaf nitrogen to phosphorus ratios of tropical trees: experimental assessment of physiological and environmental controls, New Phytol., 185, 770–779, 2010.

Collatz, G. J., Ball, J. T., Grivet, C., and Berry, J. A.: Physiological and environmental regualtion of stomatal conductance, photosynthesis, and transpiration: a model that includes a laminar boundary layer, Agr. Forest Meteorol., 54, 107–136, 1991a.

Collatz, G. J., Ball, J. T., Grivet, C., and Berry, J. A.: Physiological and environmental regulation of stomatal conductance, photosynthesis and transpiration: a model that includes a laminar boundary layer, Agr. Forest Meteorol., 54, 107–136, 1991b.

Comstock, J. and Ehleringer, J. R.: Photoperiod and photosynthetic capacity in *Lotus scoparius*, Plant Cell Environ., 9, 609–612, 1986.

Crafts-Brandner, S. J. and Law, R. D.: Effect of heat stress on the inhibition and recovery of ribulose-1,5-bisphosphate carboxylase/oxygenase activation state, Planta, 212, 67–74, 2000.

Crafts-Brandner, S. J. and Salvucci, M. E.: Rubisco activase constrains the photosynthetic potential of leaves at high temperature and CO_2, P. Natl. Acad. Sci. USA, 24, 1343–13435, doi:10.1073/pnas.230451497, 2000.

Dewar, R. C.: Maximum entropy production and plant optimization theories, Philos. Trans. R. Soc. Lond. B. Biol. Sc., 365, 1429–1435, doi:10.1098/rstb.2009.0293, 2010.

Dubois, J.-J. B., Fiscus, E. L., Booker, F. L., Flowers, M. D., and Reid, C. D.: Optimizing the statistical estimation of the parameters of the Farquhar–von Caemmerer–Berry model of photosynthesis, New Phytol., 176, 402–414, 2007.

Evans, J. R. and Poorter, H.: Photosynthetic acclimation of plants to growth irradiance: the relative importance of specific leaf area and nitrogen partitioning in maximizing carbon gain, Plant Cell Environ., 24, 755–767, 2001.

Farquhar, G. D. and von Caemmerer, S. (Eds.): Modelling of Photosynthetic Response to Environmental Conditions, Springer-Verlag, Heidelberg-Berlin-New York, 1982.

Farquhar, G. D., Von Caemmerer, S., and Berry, J.: A biochemical model of photosynthetic CO_2 assimilation in leaves of C_3 species, Planta, 149, 78–90, 1980.

Franklin, O., Johansson, J., Dewar, R. C., Dieckmann, U., McMurtrie, R. E., Brännström, Å., and Dybzinski, R.: Modeling carbon allocation in trees: a search for principles, Tree Physiol., 32, 648–666, 2012.

GMDD
8, 6217–6266, 2015

Friedlingstein, P., Meinshausen, M., Arora, V. K., Jones, C. D., Anav, A., Liddicoat, S. K., and Knutti, R.: Uncertainties in CMIP5 climate projections due to carbon cycle feedbacks, J. Climate, 27, 511–526, 2014.

Friend, A.: Use of a model of photosynthesis and leaf microenvironment to predict optimal stomatal conductance and leaf nitrogen partitioning, Plant Cell Environ., 14, 895–905, 1991.

Goll, D. S., Brovkin, V., Parida, B. R., Reick, C. H., Kattge, J., Reich, P. B., van Bodegom, P. M., and Niinemets, Ü.: Nutrient limitation reduces land carbon uptake in simulations with a model of combined carbon, nitrogen and phosphorus cycling, Biogeosciences, 9, 3547–3569, doi:10.5194/bg-9-3547-2012, 2012.

Hanson, P. J., Amthor, J. S., Wullschleger, S. D., Wilson, K. B., Grant, R. F., Hartley, A., Hui, D., Hunt, J. E. R., Johnson, D. W., Kimball, J. S., King, A. W., Luo, Y., McNulty, S. G., Sun, G., Thornton, P. E., Wang, S., Williams, M., Baldocchi, D. D., and Cushman, R. M.: Oak forest carbon and water simulations: model intercomparisons and evaluations against independent data, Ecol. Monogr., 74, 443–489, 2004.

Harley, P. C. and Baldocchi, D. D.: Scaling carbon dioxide and water vapour exchange from leaf to canopy in a decisuous forest. I, leaf model parametrization, Plant Cell Environ., 18, 1146–1156, 1995.

Harley, P. C., Thomas, R. B., Reynolds, J. F., and Strain, B. R.: Modelling photosynthesis of cotton grown in elevated CO_2, Plant Cell Environ., 15, 271–282, 1992.

Haxeltine, A. and Prentice, I. C.: A general model for the light-use efficiency of primary production, Funct. Ecol., 10, 551–561, 1996.

Houlton, B. Z., Marklein, A. R., and Bai, E.: Representation of nitrogen in climate change forecasts, Nature Clim. Change, 5, 398–401, 2015.

Hurrell, J. W., Holland, M. M., Gent, P. R., Ghan, S., Kay, J. E., Kushner, P. J., Lamarque, J. F., Large, W. G., Lawrence, D., Lindsay, K., Lipscomb, W. H., Long, M. C., Mahowald, N., Marsh, D. R., Neale, R. B., Rasch, P., Vavrus, S., Vertenstein, M., Bader, D., Collins, W. D., Hack, J. J., Kiehl, J., and Marshall, S.: The community Earth system model: a framework for collaborative research, B. Am. Meteorol. Soc., 94, 1339–1360, 2013.

Jarvis, P. G.: Coupling of carbon and water interactions in forest stands, Tree Physiol., 2, 347–368, 1986.

Jordan, D. B. and Ogren, W. L.: The CO_2/O_2 specificity of ribulose 1,5-biphosphate carboxylase/oxygenase. Dependence on ribulose-biphosphate concentration, pH and temperature, Planta, 161, 308–313, 1984.

GMDD

8, 6217–6266, 2015

Kattge, J. and Knorr, W.: Temperature acclimation in a biochemical model of photosynthesis: a reanalysis of data from 36 species, Plant Cell Environ., 30, 1176–1190, 2007.
Kattge, J., Knorr, W., Raddatz, T., and Wirth, C.: Quantifying photosynthetic capacity and its relationship to leaf nitrogen content for global-scale terrestrial biosphere models, Glob. Change Biol., 15, 976–991, 2009.
Knorr, W. and Kattge, J.: Inversion of terrestrial ecosystem model parameter values against eddy covariance measurements by Monte Carlo sampling, Glob. Change Biol., 11, 1333–1351, 2005.
Laloy, E. and Vrugt, J. A.: High-dimensional posterior exploration of hydroligic models using multiple-try DREAM($_{zs}$) and high-performance computing, Water Resour. Res., 48, W01526, doi:10.1029/2011WR010608, 2012.
Law, R. D. and Crafts-Brandner, S. J.: Inhibition and acclimation of photosynthesis to heat stress is closely correlated with activation of ribulose-1,5-bisphosphate carboxylase/oxygenase, Plant Physiol., 120, 173–181, 1999.
Leuning, R.: Modeling stomatal behavior and photosynthesis of *Eucalyptus grandis*, Aust. J. Plant Physiol., 17, 159–175, 1990.
Leuning, R.: Scaling to a common temperature improves the correlation between photosynthesis parameters J_{max} and $V_{c,max}$, J. Exp. Bot., 307, 345–347, 1997.
Leuning, R.: Temperature dependence of two parameters in a photosynthesis model, Plant Cell Environ., 25, 1205–1210, 2002.
Limousin, J.-M., Misson, L., Lavoir, A.-V., Martin, N. K., and Rambal, S.: Do photosynthetic limitations of evergreen *Quercus ilex* leaves change with long-term increased drought severity?, Plant Cell Environ., 33, 863–875, 2010.
Lin, Y.-S., Medlyn, B. E., Duursma, R. A., Prentice, I. C., Wang, H., Baig, S., Eamus, D., de Dios, V. R., Mitchell, P., Ellsworth, D. S., de Beeck, M. O., Wallin, G., Uddling, J., Tarvainen, L., Linderson, M.-L., Cernusak, L. A., Nippert, J. B., Ocheltree, T. W., Tissue, D. T., Martin-StPaul, N. K., Rogers, A., Warren, J. M., De Angelis, P., Hikosaka, K., Han, Q., Onoda, Y., Gimeno, T. E., Barton, C. V. M., Bennie, J., Bonal, D., Bosc, A., Low, M., Macinins-Ng, C., Rey, A., Rowland, L., Setterfield, S. A., Tausz-Posch, S., Zaragoza-Castells, J., Broadmeadow, M. S. J., Drake, J. E., Freeman, M., Ghannoum, O., Hutley, L. B., Kelly, J. W., Kikuzawa, K., Kolari, P., Koyama, K., Limousin, J.-M., Meir, P., Lola da Costa, A. C., Mikkelsen, T. N., Salinas, N., Sun, W., and Wingate, L.: Optimal stomatal behaviour around the world, Nature Clim. Change, 5, 459–464, doi:10.1038/nclimate2550, 2015.

GMDD
8, 6217–6266, 2015

Long, S. P., Ainsworth, E. A., Rogers, A., and Ort, D. R.: Rising atmospheric carbon dioxide: plants FACE the future, Annu. Rev. Plant Biol., 55, 591–628, 2004.
Maire, V., Martre, P., Kattge, J., Gastal, F., Esser, G., Fontaine, S., and Soussana, F.: The coordination of leaf photosynthesis links C and N fluxes in C_3 plant species, PLos ONE, 7, e38245, doi:10.1371/journal.pone.0038345, 2012.
Makino, A. and Osmond, B.: Effects of nitrogen nutrition on nitrogen partitioning between chloroplasts and mitochondria in pea and wheat, Plant Physiol., 96, 355–362, 1991.
Manter, D. K. and Kerrigan, J.: A / C_i curve analysis across a range of woody plant speices: influence of regression analysis parameters and mesophyll conductance, J. Exp. Bot., 55, 2581–2588, 2004.
Maroco, J. P., Breia, E., Faria, T., Pereira, J. S., and Chaves, M. M.: Effects of long-term exposure to elevated CO_2 and N fertilization on the development of photosynthetic capacity and biomass accumulation in *Quercus suber* L., Plant Cell Environ., 25, 105–113, 2002.
Martin, B., Martensson, O., and Öquist, G.: Seasonal effects on photosynthetic electron transport and fluorescence properties in isolated chloroplasts of *Pinus sylvestris*, Physiol. Plantarum, 44, 102–109, 1978.
Mayer, D. G. and Butler, D. G.: Statistical validation, Ecol. Model., 68, 21–32, 1993.
McDowell, N.: Mechanisms linking drought, hydraulics, carbon metabolism, and vegetation mortality, Plant Physiol., 155, 1051–1059, 2011.
Medlyn, B. E., Badeck, F.-W., De Pury, D. G. G., Barton, C. V. M., Broadmeadow, M., Ceulemans, R., De Angelis, P., Forstreuter, M., Jach, M. E., Kellomäki, S., Laitat, E., Marek, M., Philippot, S., Rey, A., Strassemeyer, J., Laitinen, K., Liozon, R., Portier, B., Proberntz, P., Wang, K., and Jarvis, P. G.: Effects of elevated $[CO_2]$ on photosynthesis in European forest species: a meta-analysis of model parameters, Plant Cell Environ., 22, 1475–1495, 1999.
Medlyn, B. E., Dreyer, E., Ellsworth, D., Forstreuter, M., Harley, P. C., Kirschbaum, M. U. F., Le Roux, X., Montpied, P., Strassemeyer, J., Walcroft, A., Wang, K., and Loustau, D.: Temperature response of parameters of a biochemically based model of photosynthesis, II, a review of experimental data, Plant Cell Environ., 25, 1167–1179, 2002a.
Medlyn, B. E., Loustau, D., and Delzon, S.: Temperature response of parameters of a biochemically based model of photosynthesis, I, Seasonal changes in mature maritime pine (*Pinus pinaster* Ait.), Plant Cell Environ., 25, 1155–1165, 2002b.

GMDD
8, 6217–6266, 2015

Medlyn, B. E., Robinson, B. A., Clement, R., and McMurtrie, R. E.: On the validation of models of forest CO_2 exchange using eddy covariance data: some perils and pitfalls, Tree Physiol., 25, 839–857, 2005.

Medlyn, B. E., Duursma, R. A., Eamus, D., Ellsworth, D. A., Prentice, I. C., Barton, C. V. M., Crous, K. Y., De Angelis, P., Freeman, M., and Wingate, L.: Reconciling the optimal and empirical approaches to modelling stomatal conductance, Glob. Change Biol., 10, 1365–2486, 2011.

Meehl, G. A., Boer, G. J., Covey, C., Latif, M., and Stouffer, R. J.: The coupled model intercomparison project (CMIP), B. Am. Meteorol. Soc., 81, 313–318, 2000.

Miao, Z., Xu, M., Lathrop, R. G., and Wang, Y.: Comparison of the A–Cc curve fitting methods in determining maximum ribulose 1· 5-bisphosphate carboxylase/oxygenase carboxylation rate, potential light saturated electron transport rate and leaf dark respiration, Plant Cell Environ., 32, 109–122, 2009.

Moorcroft, P. R., Hurtt, G. C., and Pacala, S. W.: A method for scaling vegetation dynamics: the ecosystem demography model (ED), Ecol. Monogr., 71, 557–586, 2001.

Niinemets, Ü., and Tenhunen, J. D.: A model separating leaf structural and biphysiological effects on carbon gain along light gradients for the shade-tolerant species *Acer saccharum*, Plant Cell Environ., 20, 845–866, doi:10.1046/j.1365-3040.1997.d01-133.x, 1997.

Oleson, K. W., Lawrence, D. M., Bonan, G. B., Drewniak, B., Huang, M., Koven, C. D., Levis, S., Li, F., Riley, W. J., Subin, Z. M., Swenson, S. C., Thornton, P. E., Bozbiyik, A., Fisher, R., Kluzek, E., Lamarque, J.-F., Lawrence, P. J., Leung, L. R., Lipscomb, W., Muszala, S., Ricciuto, D. M., Sacks, W., Sun, Y., Tang, J., and Yang, Z.-L.: Technical Description of version 4.5 of the Community Land Model (CLM). NCAR Technical Note NCAR/TN-503+STR, National Center for Atmospheric Research, Boulder, CO, 2013.

Öquist, G., Brunes, L., Hällgren, J.-E., Gezelius, K., Hallén, M., and Malmberg, G.: Effects of artificial frost hardening and winter stress on net photosynthesis, photosynthetic electron transport and RuBP carboxylase activity in seedlings of *Pinus sylvestris*, Physiol. Plantarum, 48, 526–531, 1980.

Prentice, I. C., Dong, N., Gleason, S. M., Maire, V., and Wright, I. J.: Balancing the costs of carbon gain and water transport: testing a new theoretical framework for plant functional ecology, Ecol. Lett., 17, 82–91, 2014.

GMDD

8, 6217–6266, 2015

Raddatz, T., Reick, C., Knorr, W., Kattge, J., Roeckner, E., Schnur, R., Schnitzler, K. G., Wetzel, R. G., and Jungclaus, J.: Will the tropical land biosphere dominate the climate-carbon cycle feedback during the twenty-first century?, Clim. Dynam., 29, 565–574, 2007.
Reich, P. B. and Oleksyn, J.: Global patterns of plant leaf N and P in relation to temperature and latitude, P. Natl. Acad. Sci. USA, 101, 11001–11006, 2004.
Reich, P. B., Kloeppel, B. D., Ellsworth, D., and Walters, M. B.: Different photosynthesis nitorgen relations in decidious hardwood and evergreen coniferous tree species, Oecologia, 104, 24–30, 1995.
Reich, P. B., Walters, M. B., Tjoelker, M. G., Vanderklein, D., and Buschena, C.: Photosynthesis and respiration rates depend on leaf and root morphology and nitrogen concentration in nine boreal tree species differing in relative growth rate, Funct. Ecol., 12, 395–405, 1998.
Riebeek, H.: The Carbon Cycle, NASA Earth Observatory, availble at: http://earthobservatory.nasa.gov/Features/CarbonCycle/ (last access: 1 June 2015), 2011.
Ripullone, F., Grassi, G., Lauteri, M., and Borghetti, M.: Photosynthesis–nitrogen relationships: interpretation of different patterns between *Pseudotsuga menziesii* and *Populus* x *euroamericana* in a mini-stand experiment, Tree Physiol., 23, 137–144, 2003.
Rogers, A.: The use and misuse of $V_{c,max}$ in earth system models, Photosynth. Res., 119, 1–15, 2014.
Ryan, M. G.: Foliar maintenance respiration of subalpine and boral trees and shrubs in relation to nitrogen concentration, Plant Cell Environ., 18, 765–772, 1995.
Schaefer, K., Schwalm, C. R., Williams, C., Arain, M. A., Barr, A., Chen, J. M., Davis, K. J., Dimitrov, D., Hilton, T. W., Hollinger, D. Y., Humphreys, E., Poulter, B., Raczka, B. M., Richardson, A. D., Sahoo, A., Thornton, P., Vargas, R., Verbeeck, H., Anderson, R., Baker, I., Black, T. A., Bolstad, P., Chen, J., Curtis, P. S., Desai, A. R., Dietze, M., Dragoni, D., Gough, C., Grant, R. F., Gu, L., Jain, A., Kucharik, C., Law, B., Liu, S., Lokipitiya, E., Margolis, H. A., Matamala, R., McCaughey, J. H., Monson, R., Munger, J. W., Oechel, W., Peng, C., Price, D. T., Ricciuto, D., Riley, W. J., Roulet, N., Tian, H., Tonitto, C., Torn, M., Weng, E., and Zhou, X.: A model-data comparison of gross primary productivity: results from the North American Carbon Program site synthesis, J. Geophys. Res.-Biogeo., 117, G03010, doi:10.1029/2012JG001960, 2012.
Schymanski, S. J., Sivapalan, M., Roderick, M. L., Hutley, L. B., and Beringer, J.: An optimality-based model of the dynamic feedbacks between natural vegetation and the water balance, Water Resour. Res., 45, W01412, doi:10.1029/2008WR006841, 2009.

GMDD
8, 6217–6266, 2015

Sellers, P. J., Dickinson, R., Randall, D. A., Betts, A. K., Hall, F. G., Berry, J. A., Collatz, G. J., Denning, A. S., Mooney, H. A., Nobre, A. D., Sato, N., Field, C. B., and HendersonSellers, A.: Modeling the exchanges of energy, water, and carbon between continents and the atmosphere, Science, 275, 502–509, 1997.

Smith, E.: The influence of light and carbon dioxide on photosynthesis, General Physiology, 20, 807–830, 1937.

Song, Y. H., Ito, S., and Imaizumi, T.: Flowering time regulation: photoperiod- and temperature-sensing in leaves, Trends Plant Sci., 18, 575–583, 2013.

Spreitzer, R. J. and Salvucci, M. E.: Rubisco: structure, regulatory interactions, and possibilities for a better enzyme, Annu. Rev. Plant Biol., 53, 449–475, 2002.

Strand, M. and Öquist, G.: Effects of frost hardening, dehardening and freezing trees on in vivo fluorescence of seedlings of Scots pine (*Pinus sylvestris* L.), Plant Cell Environ., 11, 231–238, 1988.

Taylor, K. E., Stouffer, R. J., and Meehl, G. A.: An overview of CMIP5 and the experiment design, B. Am. Meteorol. Soc. , 93, 485–498, 2013.

Thomas, R. Q. and Williams, M.: A model using marginal efficiency of investment to analyze carbon and nitrogen interactions in terrestrial ecosystems (ACONITE Version 1), Geosci. Model Dev., 7, 2015–2037, doi:10.5194/gmd-7-2015-2014, 2014.

Van Oijen, M., Schapendonk, A., and Hoglind, M.: On the relative magnitudes of photosynthesis, respiration, growth and carbon storage in vegetation, Ann. Bot.-London, 105, 793–797, 2010.

Walker, A. P., Beckerman, A. P., Gu, L., Kattge, J., Cernusak, L. A., Domingues, T. F., Scales, J. C., Wohlfahrt, G., Wullschleger, S. D., and Woodward, F. I.: The relationship of leaf photosynthetic traits – Vc,max and Jmax – to leaf nitrogen, leaf phosphorus, and specific leaf area: a meta-analysis and modeling study, Ecology and Evolution, 4, 3218–3235, 2014.

Wang, Y. P., Law, R. M., and Pak, B.: A global model of carbon, nitrogen and phosphorus cycles for the terrestrial biosphere, Biogeosciences, 7, 2261–2282, doi:10.5194/bg-7-2261-2010, 2010.

White, M. A., Thornton, P. E., Running, S. W., and Nemani, R. R.: Parameterization and sensitivity analysis of the BIOME-BCG terrestrial ecosystem model: net primary production controls, Earth Interact., 4, 1–85, 2000.

GMDD
8, 6217–6266, 2015

Whitley, R. J., Catriona, M. O., Macinnis-Ng, C., Hutley, L. B., Beringer, J., Zeppel, M., Williams, M., Taylor, D., and Eamus, D.: Is productivity of mesic savannas light limited or water limited? Results of a simulation study, Glob. Change Biol., 17, 3130–3149, 2011.

Wieder, W. R., Cleveland, C. C., Lawrence, D. M., and Bonan, G. B.: Effects of model structural uncertainty on carbon cycle projections: biological nitrogen fixation as a case study, Environ. Res. Lett., 10, 044016, doi:10.1088/1748-9326/10/4/044016, 2015.

Wilson, K. B., Baldocchi, D. D., and Hanson, P. J.: Leaf age affects the seasonal pattern of photosynthetic capacity and net ecosystem exchange of carbon in a deciduous forest, Plant Cell Environ., 24, 571–583, 2001.

Wright, I. J., Reich, P. B., Westoby, M., Ackerly, D. D., Baruch, Z., Bongers, F., Cavender-Bares, J., Chapin, T., Cornelissen, J. H. C., Diemer, M., Flexas, J., Garnier, E., Groom, P. K., Gulias, J., Hikosaka, K., Lamont, B. B., Lee, T. D., Lee, W., Lusk, C. H., Midgley, J. J., Navas, M.-L., Niinemets, Ü., Olesksyn, J., Osada, N., Poorter, H., Poot, P., Prior, L., Pyankov, V. I., Roumet, C., Thomas, S. C., Tjoelker, M. G., Veneklaas, E. J., and Villar, R.: The worldwide leaf economics spectrum, Nature, 428, 821–827, 2004.

Wullschleger, S. D.: Biochemical limitations to carbon assimilation in C_3 plants: a retrospective analysis of A / C_i curves from 109 species, J. Exp. Bot., 44, 907–920, 1993.

Xu, C., Fisher, R., Wullschleger, S. D., Wilson, C. J., Cai, M., and McDowell, N.: Toward a mechanistic modeling of nitrogen limitation on vegetation dynamics, PLos ONE, 7, e37914, doi:10.1371/journal.pone.0037914, 2012.

Xu, L. and Baldocchi, D. D.: Seasonal trends in photosynthetic parameters and stomatal conductance of blue oak (*Quercus douglasii*) under prolonged summer drought and high temperature, Tree Physiol., 23, 865–877, 2003.

Yamori, W., Suzuki, K., Noguchi, K. O., Nakai, M., and Terashima, I.: Effects of Rubisco kinetics and Rubisco activation state on the temperature dependence of the photosynthetic rate in spinach leaves from contrasting growth temperatures, Plant Cell Environ., 29, 1659–1670, 2006.

GMDD
8, 6217–6266, 2015

Table 1. Mean values of parameters obtained by using the Differential Evolution Adaptive Metropolis Snooker updater (DREAM-ZS) sampling technique when TRF1 and TRF2 were used. TRF1 was a temperature response function that considered the potential for acclimation to growth temperature while TRF2 was a temperature response function that did not consider change in temperature response coefficients to growth temperature. The parameters include; $J_{\mathrm{max}b0}$ (unitless) – baseline proportion of nitrogen allocated for electron transport rate, $J_{\mathrm{max}b1}$ (unitless) – electron transport rate response to light availability, $t_{\mathrm{c},j0}$ (unitless) – baseline ratio of Rubisco limited rate to light limited rate, and H (unitless) – electron transport rate response to relative humidity. The standard deviations are shown in the parentheses.

Statistics	$J_{\mathrm{max}b0}$	$J_{\mathrm{max}b1}$	$t_{\mathrm{c},j0}$	H
TRF1	0.0311 (0.0004)	0.1745 (0.0002)	0.8054 (0.0015)	6.0999 (0.2416)
TRF2	0.0322 (0.0002)	0.1695 (0.0006)	0.7760 (0.0031)	5.7139 (0.0354)

GMDD
8, 6217–6266, 2015

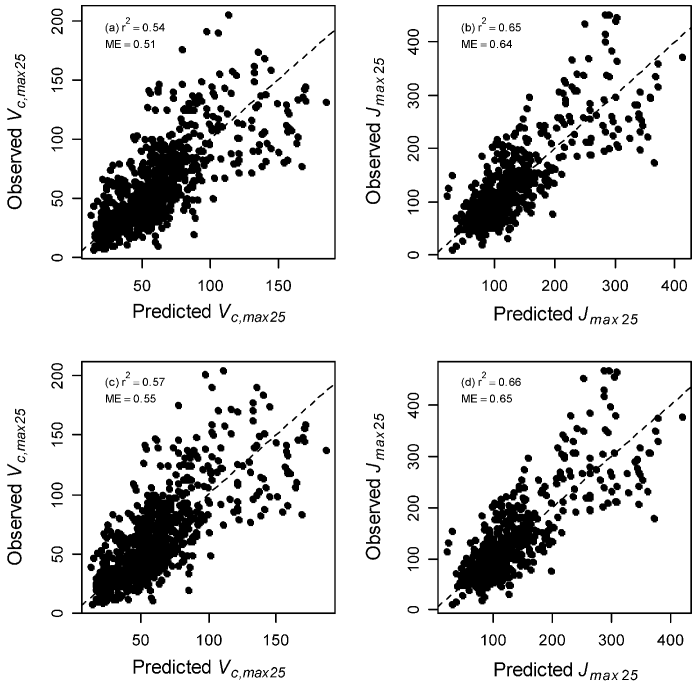

Figure 1. Percentage of variations (r^2, ME; model efficiency) in observed $V_{c,max25}$ (µmol CO_2 m^{-2} s^{-1}) explained by modeled $V_{c,max25}$ **(a, c)** and in observed J_{max25} (µmol electron m^{-2} s^{-1}) explained by modeled J_{max25} **(b, d)** across all of the species, using TRF1 **(a, b)** and TRF2 **(c, d)**, where the nitrogen allocation model, the environmental variables, leaf mass per leaf area, and the leaf nitrogen contents were used. TRF1 was a temperature response function that considered the potential for acclimation to growth temperature while TRF2 was a temperature response function that did not consider change in temperature response coefficients to growth temperature. The r^2 is derived by a linear regression between observed and modeled values. The dashed line is the 1 : 1 line.

GMDD
8, 6217–6266, 2015

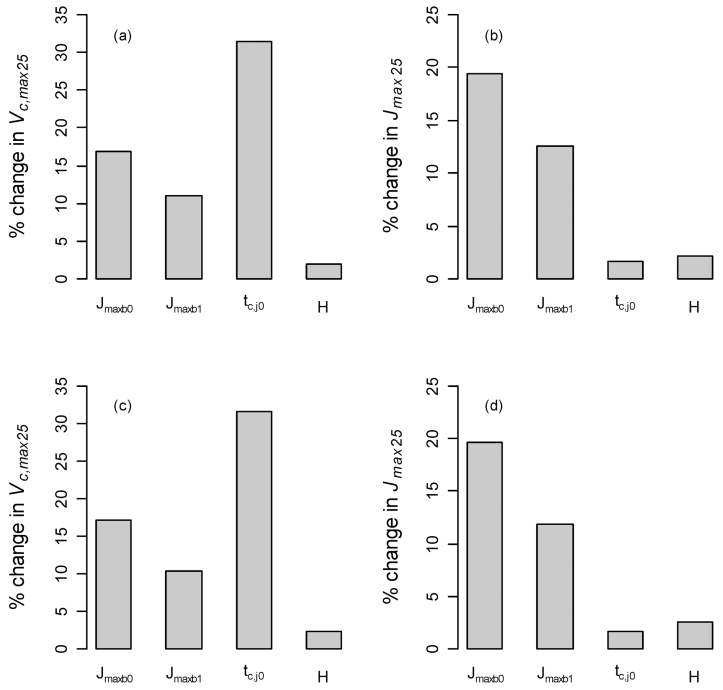

Figure 2. Effects of changes in nitrogen allocation parameters on the predicted $V_{c,max25}$ (µmol CO_2 m^{-2} s^{-1}) **(a, c)** and J_{max25} (µmol electron m^{-2} s^{-1}) **(b, d)**. Each parameter (J_{maxb0}, J_{maxb1}, $t_{c,j0}$, and H) was varied one at a time by ±15 % of its value by using either TRF1 **(a, b)** or TRF2 **(c, d)**. TRF1 was a temperature response function that considered the potential for acclimation to growth temperature while TRF2 was a temperature response function that did not consider change in temperature response coefficients to growth temperature. The environmental variables (day length: 14 h, daytime radiation: 182 W m^{-2}, temperature: 14 °C, relative humidity: 0.6 (unitless), and carbon dioxide: 393 ppm) were held fixed. Firstly, $V_{c,max25}$ and J_{max25} values were obtainedS at changed parameter value. Next, percentage changes in $V_{c,max25}$ and J_{max25} were calculated relative to the baseline values of $V_{c,max25}$ and J_{max25}.

GMDD
8, 6217–6266, 2015

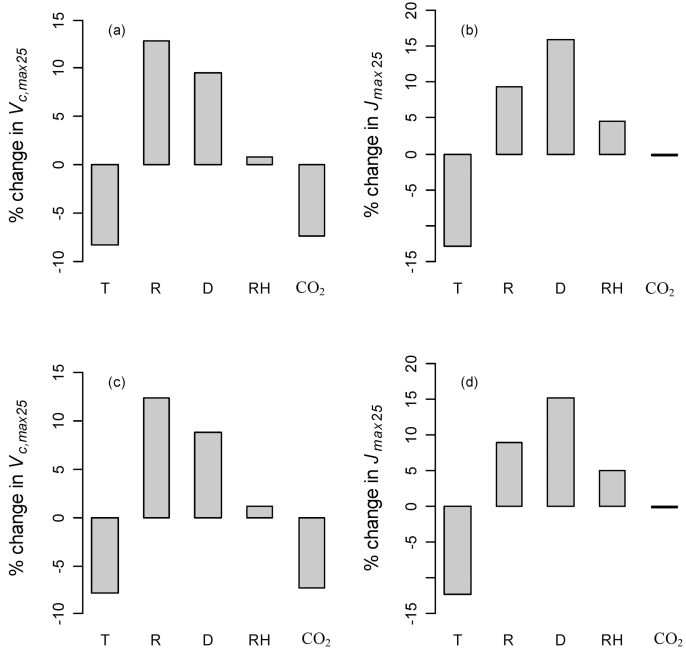

Figure 3. Effects of environmental variables (day length, daytime radiation, temperature, relative humidity, and carbon dioxide) on predicted $V_{c,max25}$ (µmol CO_2 m^{-2} s^{-1}) **(a, c)** and J_{max25} (µmol electron m^{-2} s^{-1}) **(b, d)**. Each environmental variable (day length: 14 h, daytime radiation; 182 W m^{-2}, temperature; 14 °C, relative humidity; 0.6 (unitless), and carbon dioxide; 393 ppm) was varied one at a time by ±15 %. TRF1 **(a, b)** and TRF2 **(c, d)** were used, with the parameters (J_{maxb0}, J_{maxb1}, $t_{c,j0}$, and H) being held fixed. TRF1 was a temperature response function that considered the potential for acclimation to growth temperature while TRF2 was a temperature response function that did not consider change in temperature response coefficients to growth temperature. Firstly, $V_{c,max25}$ and J_{max25} values were obtained at changed environmental condition. Next, percentage changes in $V_{c,max25}$ and J_{max25} were calculated relative to the baseline values of $V_{c,max25}$ and J_{max25}.

GMDD
8, 6217–6266, 2015

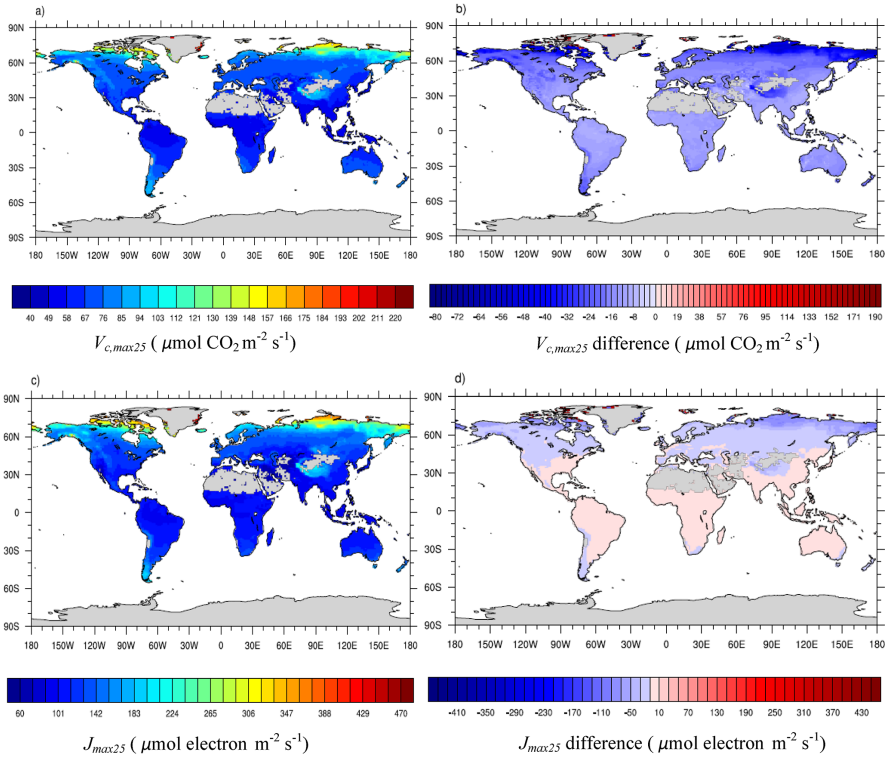

Figure 4. Summer season photosynthetic capacity for the top leaf layer in the canopy ($V_{c,max25}$; μmol CO_2 m^{-2} s^{-1}, **a**; J_{max25}; μmol electron m^{-2} s^{-1}, **c**) under historical climatic conditions and the difference in either $V_{c,max25}$ **(b)** or J_{max25} **(d)** due to changed climatic conditions. Difference in the photosynthetic capacity was calculated as that under future climate minus that under historical climate. Ten-year monthly averages of climatic conditions for the past (1995–2004) and the future (2090–2099) were used to drive the model. The model was run by using TRF1, which was a temperature response function that considered the potential for acclimation to growth temperature.

GMDD
8, 6217–6266, 2015

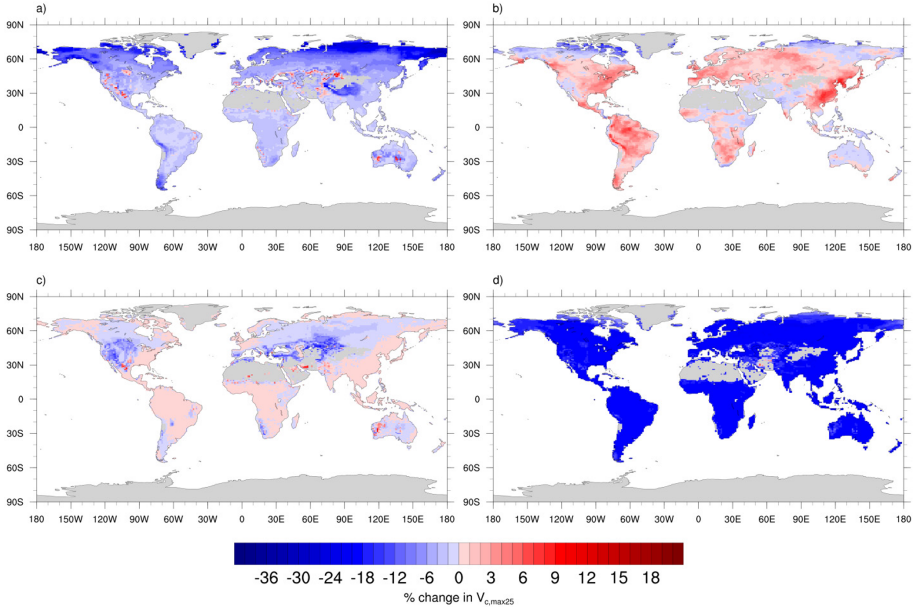

Figure 5. Sensitivity of $V_{c,max25}$ (µmol CO_2 m^{-2} s^{-1}) to changes in environmental variables (**a**: Temperature, **b**: Radiation, **c**: Humidity, and **d**: CO_2) at the global scale by using TRF1. TRF1 was a temperature response function that considered the potential for acclimation to growth temperature. The changes in environmental conditions are based on 10 year monthly averages of climatic conditions for the past (1995–2004) and the future (2090–2099).

GMDD
8, 6217–6266, 2015

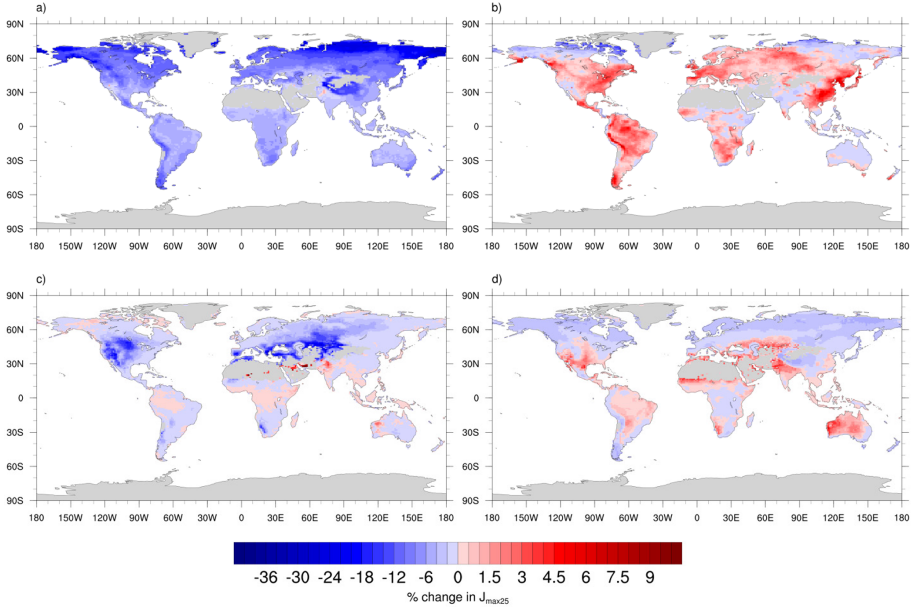

Figure 6. Sensitivity of J_{max25} (µmol electron $m^{-2} s^{-1}$) to changes in environmental variables (**a**: Temperature, **b**: Radiation, **c**: Humidity, and **d**: CO_2) at the global scale using TRF1. TRF1 was a temperature response function that considered the potential for acclimation to growth temperature. The changes in environmental conditions are based on 10 year monthly averages of climatic conditions for the past (1995–2004) and the future (2090–2099).

GMDD
8, 6217–6266, 2015

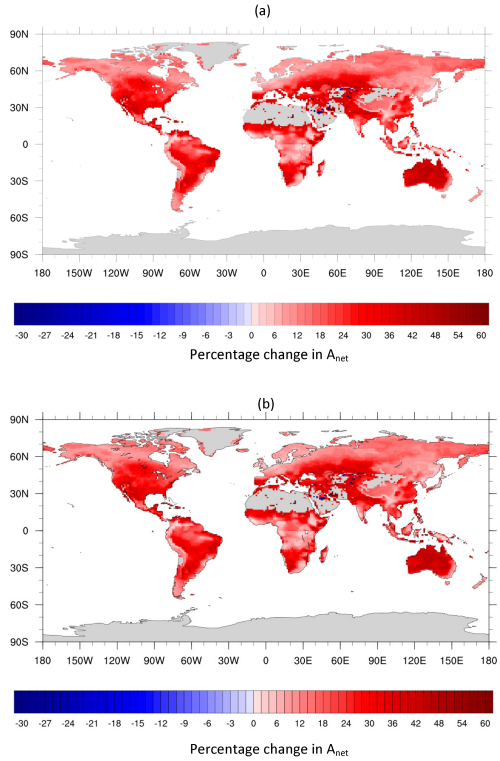

Figure 7. Percentage differences in A_{net} (µmol CO_2 $m^{-2}s^{-1}$) for using $V_{c,max25}$ (µmol CO_2 $m^{-2}s^{-1}$) and J_{max25} (µmol electron $m^{-2}s^{-1}$) based on historical climate and that using $V_{c,max25}$ and J_{max25} based on future climate conditions. TRF1 **(a)** and TRF2 **(b)** were used in the model simulations. TRF1 was a temperature response function that considered the potential for acclimation to growth temperature while TRF2 was a temperature response function that did not consider change in temperature response coefficients to growth temperature. 10 year monthly averages of climatic conditions for the past (1995–2004) and the future (2090–2099) were used to drive the model.

GMDD
8, 6217–6266, 2015